UCLouvain

École polytechnique de Louvain

# Sensorimotor control of bird flight

Author : **Caroline Boggis**
Supervisor : **Renaud Ronsse**
Readers : **Gianmarco Ducci, Greet Kerckhofs**
Academic year 2020–2021
Master [120] in Mechanical Engineering

# Aknowledgements

I am very grateful for the discoveries and lessons I made during this master thesis. I really think that they will serve me well in the future.

I would like to thank my supervisor Professor Renaud Ronsse for his support, his great availability and our insightful conversations.

I would like to thank Gianmarco Ducci, the PhD student who supervised me, for his great help when I was facing difficulties, his availability and his encouragements.

A special thank you to Professor Greet Kerckhofs who kindly accepted to be part of my master thesis jury and to read this master thesis.

I would like to express my gratitude to my family and my friends for their mental support during my studies and during this master thesis. A special thank you to my friend Henri who particularly supported me.

# Contents

# 1 Introduction

This master thesis is part of the RevealFlight Project which is a research project of Ecole Polytechnique de Louvain. This Project aims at studying optimisation mechanisms deployed by biological flyers, in particular migratory birds. Migratory birds were chosen for their impressive flight stability and flight optimisation capabilities. The objective is to provide a better understanding of bird flight mechanics by studying aerodynamics, biomechanics and sensorimotor control. The specificity of this project is to study the interconnection between these aspects.

The RevealFlight Project studies bird morphology as a frame, neuro-muscular configuration as an actuation layer that realises the bird gait, flapping wing beats which generate the lift force, feathers and wing compliance as flow control mechanisms and flight formations of migratory birds as efficiency gain mechanisms. All this is studied in an unified framework combining biomechanical, sensory, aerodynamic and social interaction models.

This is a brief summary of the presentation of the project which is explained in more detail at the address [1].

This master thesis will focus on the sensorimotor control of bird flight. The objective is to implement a feedback loop which restores flight stability when a source of instability occurs, by designing a controller. Instability may be induced by a change of direction or magnitude of wind stresses.

First, a focus will be done on migratory bird's sensory system, in particular on sensory receptors. The aim is to identify relevant sensory receptors which are able to give the sensory data needed for the bird to adapt its flight parameters to stall onset.

Then, the problem statement will be presented and will ask the main research questions.

Next, the bird model will be presented. This model was implemented by Gianmarco Ducci, PhD at Ecole Polytechnique de Louvain, and is accessible at the address [2]. The objective of this master thesis is to design a controller to stabilise the bird flight in this model.

After that, the designed controller will be presented: firstly, by its design steps, secondly, by the explanation of its implementation.

Finally, the results of the influence of the controller on flight stability will be displayed and discussed.

# 2 Bird sensory system

## 2.1 Functioning of sensory system

The sensory nervous system is a part of the nervous system which processes sensory information. It responds to the need for an organism to be able to perceive, process and integrate stimuli from the environment. Sensory receptors give information about the environment, it may be information of light, sound, smell, taste and somatic sensation (which includes touch, pain, pressure, vibration, heat and cold). In the case of migratory birds, there is also the ability to sense geomagnetic fields. [3]

As can be seen on figure 2.1, if a sensory receptor from the skin, muscles or tendons of an animal detects a somatic change (onset of pain or temperature variation, for example), it transmits an impulse to the brain. The impulse travels along an afferent sensory nerve to a nerve cell of the spinal chord through a synapse. Then, it is sent up to the thalamus processing sensory signals. Next, the impulse crosses a synapse towards nerve fibers which carry the impulse to the sensory cortex of the cerebrum interpreting sensory signals. If the animal wants to initiate a movement in response, the motor cortex generates an impulse which is sent down through a nerve of the spinal chord to an efferent motor nerve. At the neuromuscular junction, the impulse crosses from the motor nerve to receptors on the motor end plate of the muscle where the muscle is stimulated.

This path is shorter in the case of a reflex arc which is a neural pathway which control reflexes. A reflex is an automatic and fast response to a stimulation. Two types of reflex arcs can be distinguished: cerebral reflex (whose integrating centre is located in the brain) and spinal reflex (whose integrating centre is located in the spine, presented on figure 2.2). In the case of vertebrates, most reflexes are spinal reflexes, their neural path is shorter than cerebral reflexes, thus it allows faster reactions. An other distinction can be made for reflex arcs: they are called autonomic if they affect inner organs and somatic if they affect muscles.

In the case of a bird in flight, the initiation of a movement could be to adjust its trajectory, speed of wing beats and angles of bones and feathers, in response to a change of direction or magnitude of the wind measured by somatic biosensors. It may be a reflex or a conscious reaction, according to the circumstances.

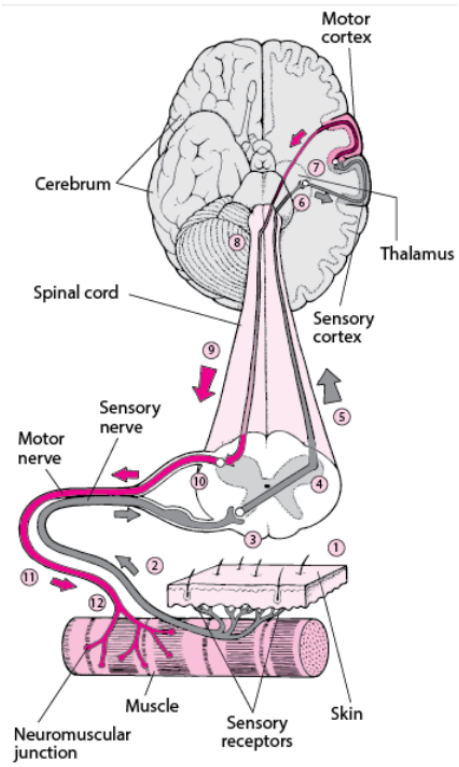


**Figure 2.1:** *Peripheral nervous system [4]*

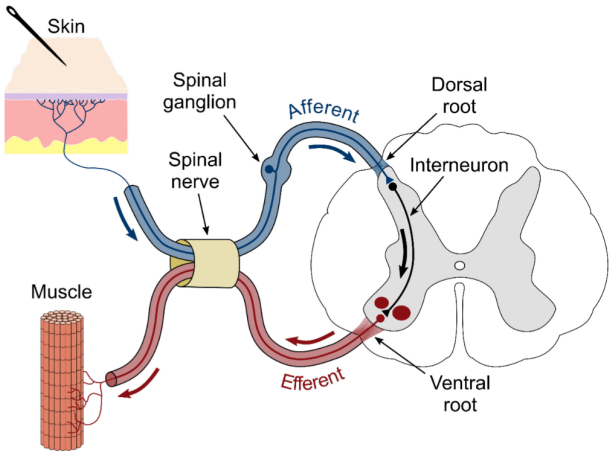


**Figure 2.2:** *Spinal reflex arc [5]*

## 2.2 Literature review on sensory receptors

In vertebrates, the main types of external sensory receptors are olfactory receptors (activated by odour molecules in the air), gustatory receptors (detecting the chemicals in food), photoreceptors (converting light into electrical signals), hair cells (converting sound pressure waves into electrical signals), thermoreceptors (detecting temperature changes in the environment), mechanoreceptors (detecting changes in pressure or mechanical stresses) and proprioreceptors (communicating information about the position of body parts). The main types of internal sensory receptors are peripheral chemoreceptors (detecting changes in blood chemical properties, such as proportion of oxygen) and nocireceptors (detecting pain).

The objective of this chapter is to identify relevant sensory receptors to model a feedback loop to stabilise flapping flight. The receptors of interest are those permitting to get an order of magnitude for pressure, speed and direction of the wind. Therefore, a focus will be done on somatic sensory receptors.

There are different levels of sensory control in flight : reflexes to environment changes, route planning and navigation. We will mainly focus on reflexes to environment changes.

Somatosensory feedback provides information about forces acting on the body, the wings and the feathers. Vestibular system provides sensory information about body accelerations. Vision provides information for flight stabilisation, trajectory control and navigation. Baroreception (blood pressure sensory system) and magnetoreception (detection of the magnitude and/or direction of magnetic fields) also provide information about navigation. Thus, we will mainly focus on somatosensory and vestibular feedback. [6]

### 2.2.1 Mechanoreceptors

In a bird skin, the mechanosensation (transduction of mechanical stimuli to neural signals) is very fast, thus it permits to the bird to quickly adapt its flight to the magnitude and direction changes of the wind. The mechanosensory system uses reflexes, thus some time is saved by bypassing the decision-making process in the brain and it reduces the reaction times. Mechanosensation is made possible by mechanoreceptors that detect changes in pressure and mechanical stresses. [6]

In vertebrates, there are four main types of mechanoreceptors : two types of rapidly-adapting receptors : Meissner corpuscles (for low frequency vibrations and fine touch) and Pacinian corpuscles (for high frequency vibrations and deep pressure), and two types of slow-adapting receptors: Merkel cells (sensitivity to light touch) and Ruffini endings (sensitivity to skin stretch).

In birds, there are also Herbst corpuscles that are quite similar to Panician corpuscles but can respond to stimuli at higher frequencies. Herbst corpuscles seem to be responsible for sensing flow disturbances, by sensing high frequency vibrations. Birds can detect the pressure changes in the air over wider range of frequencies than in water or on land because the air has a lower viscosity. [6] Most areas of the bird's body are equipped with Herbst corpuscles [7].

In the case of Eurasian siskins (which are small migratory birds), some Herbst corpuscles were found at the base of breast feathers which work as an air-current sense organ. This organ has two functions : initiating flight and inhibiting the motor output in a process of negative feedback loop for flight control, for energy consumption purposes (which are essential for migratory birds). [8]

In the case of pigeons, very numerous Herbst corpuscles were found in the wings, with a preferred orientation parallel or at right angles to primary feather (presented on figure 2.3) follicles [9]. These Herbst corpuscles react with extreme sensibility to accelerations and seem to work as a flight control system. Very few Herbst corpuscles are specialised in high frequencies (800-900 Hz against 200-400 Hz for best frequencies). [10]

It is thought that the greatest number of Herbst corpuscles from the wings analyses the air current during classical flight conditions, whereas the very few specialised in high frequencies analyse turbulences at higher frequencies and break-aways of the air stream from the wing surface (which generates high frequency vibrations). The vibrational sensitivity was studied by controlling the heart rate of pigeons subjected to vibrational stimuli. [10]

It is believed that Merkel cells and Ruffini endings are responsible for sensing wind speed and stall, by sensing feather and skin deformations due to the air [6].

It has been shown [7] that some slowly and rapidly adapting mechanoreceptors, located within the supporting tissues of the alula joint and at the base of the covert feathers (presented on figure 2.3), are responsible for detecting the approach of stall. Stall is a reduction in the lift coefficient generated by a foil (here the wings of the bird) when the critical angle of attack is exceeded [11]. These mechanoreceptors are activated by the elevation of feathers angle which leads to the alula extension. The alula is a small structure located at the joint between the hand-wing and arm-wing of birds. It is passively extended in slow flight with high angles of attack such as landing. Its function is to increase lift and delay stall. [12]

It has also been shown [7] that some slowly and rapidly adapting mechanoreceptors are responsible for detecting vibrations which permit to estimate airflow velocity. They are located within follicles of filoplume attached to the secondary flight feathers follicles (presented on figure 2.3).

A follicle is a small spherical group of cells enclosing an anatomical cavity containing other structure grows or other material [13]. Filoplumes are hairlike feathers with a few soft barbs near the tip [14] that may sense disorders of the plumage [15].

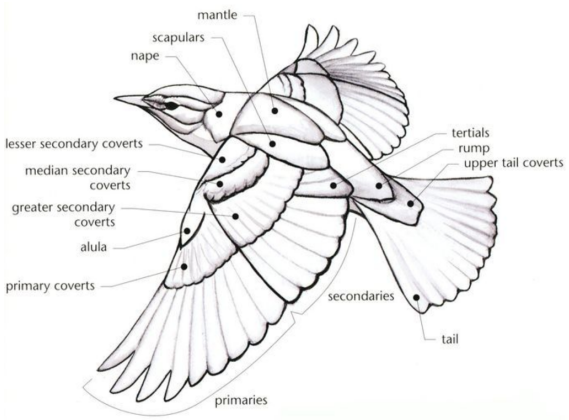


**Figure 2.3:** *Bird plumage [16]*

In the covert feathers of the dorsal wing (presented on figure 2.3), there are mechanoreceptors which detect dorsal feather elevation. Some are located on covert follicles and others are located midway between follicles. These receptors likely provide data that allow the central nervous system of the bird to detect the intensity of stall and the positions of stalled areas. [7]

It has been demonstrated that neurons in the radial nerve emit a response which is proportional to increases and deviations of airspeed over the wings. [7] It implies that some mechanoreceptors send sensory signals to inform an integrating centre of airspeed variations. It has been shown [9] that the leading edge of the wing (innervated by the radial nerve) and the leading edge of the alula (with an exceptional density of Herbst corpuscles) are the first wing structures exposed to air currents that may change continuously during flapping flight.

### 2.2.2 Vestibular reflexes

In vertebrates, the vestibular system is a sensory system which is in charge of the sense of balance and the spatial orientation to coordinate motions. It is a part of the labyrinth of the inner ear and has two components : the semicircular canals (indicating rotational movements) and the otoliths (indicating linear accelerations).

Experimentally, it was found that keeping its head fixed with respect to the horizon is necessary for a bird to be able to fly. Flight often leads to extreme linear and angular displacements of the bird's body. Keeping its head fixed permits to isolate the head from the accelerations due to flight, thanks to cervical reflexes. These accelerations are due to gravity (downwards) and due to lift (upwards), and cause oscillations approximately ten times a second (typical wingbeat frequency). Such rapidly alternating accelerations affect a lot vision and static equilibrium. Experiments with pigeons wearing collars inhibiting them from moving their heads suggest that isolating visual and vestibular systems is necessary to control flapping flight. Isolating the head permits to the eyes to focus on useful information about the bird path and position in space. [17]

There are two types of vestibular reflexes for the head : the Vestibular Ocular Reflex (VOR) and the Vestibular Collic Reflex (VCR). VOR is a reflex that coordinates eye and head movements in order to keep an object in focus (head movements must be compensated immediately by eye

movements in order to have a stabilised vision). VCR is a reflex that acts on the neck musculature in order to stabilise the head. These reflexes are essential to stabilise the vision of the bird in flight.

It has been shown that if a pigeon is suspended in a wind tunnel, it automatically extends its legs backwards, as it does during flight, when the wind exceeds a threshold value. In addition, the vestibular labyrinth is stimulated and induces extension of the wing and steering movements of the wing and the tail. Thereby, the vestibular and visual systems are coupled to the wing and tail muscles. In the wind tunnel, it is not necessary to blow at the whole pigeon, blowing toward the breast feathers on the ventral side of the pigeon is sufficient. [18]

### 2.2.3 Photoreceptors and visual reflexes

Bird photoreceptors allow them to detect visible and ultraviolet light, and light polarisation [19]. By their light polarisation sensivity, birds can use polarised light at sunset and sunrise as calibration points for a sun-based compass to assume their geographical position. The retina of birds are equipped with four types of cones for processing colour information, and double cones for processing achromatic motion and luminance variations. [6]

It has been shown that optic flow fields guide birds locomotion, as they enable to deduce both the direction of travel and time to contact. [20]. Optic flow is the apparent movement of objects, surfaces and contours in a visual scene, caused by the relative movement between an observer and what he sees [21]. The advantage of optic flow fields, compared to classical vision, is that they don't require high visual resolution, so they can be processed faster [20].

An experiment made on budgerigars showed that, in narrow passages, they were always steering such that their two eyes experience similar optic flow (similar rate of image motion). When they fly closer to one wall, the corresponding eye experience a greater magnitude of optic flow than the other one. This imbalance causes the bird to veer closer to the centre of the passage where the balance between the two optic flows is restored. This shows that birds can negotiate narrow gaps safely by balancing the speeds of image motion that are collected by the two eyes. [22]

It was also observed that an increase in the magnitude of optic flow implies a decrease of the budgerigars speed and that a decrease in the magnitude of optic flow implies an increase of the budgerigars speed. Thus, it shows that the speed of flight is regulated by monitoring the speed of image motion that is collected by the two eyes. [22]

### 2.2.4 Sensory receptors involving other systems

Migratory birds use several cues for orientation purposes : celestial cues (stars, sun, skylight polarisation pattern) and geomagnetic cues (whose reference is Earth geomagnetic field). [23] Behavioural studies showed that birds appear to perceive the magnetic field as a vector without polarity and distinguish the pole from the Equator, rather than the north and south poles. [19] However, the structure and mechanism of magnetoreceptors are still unknown.

Several nocturnal species use olfactory information for orientation. [19]

In flight, the ability to sense pressure is necessary to estimate the altitude, as altimeters for aicrafts. If it is sensitive enough, the rate of climb or descent can be determined from pressure

information alone, which can be very useful in heavy cloud cover. [24]

In birds, the innear hear has two functions : hearing (taking place in the cochlear organ) and equilibrium (taking place in the vestibular organ). Birds can hear sounds and detect infrasounds. More specifically, they can obtain directional information by flying in a circle and detecting the resulting Doppler effect (thus the change in frequency of the wave) as they fly towards and then away from an infrasound source. [19]

## 2.3 Selection of sensory receptors which are relevant for sensory feedback in flight

During a flight, the environmental conditions are continuously changing. For instance, there may be turbulence, gusts of wind or disturbances of the air current. Thus, birds have to constantly adjust their flight parameters : their angle of attack, flapping amplitude and frequency, pitch angle of the wing, spreading of single or groups of feathers, position of the alula, wing shape and wing area exposed to the wind.

To ensure flight stability, the most important feature of the airflow to determine is stall onset, that is to say its intensity and the positions of stalled areas. Stall onset is essential to determine, because it corresponds to a reduction of lift that leads to a decrease of altitude which may lead to the end of flight. Therefore, the mechanoreceptors located within the supporting tissues of the alula joint and in the covert feathers of the dorsal wing are relevant to study.

Stall onset is usually defined as occurring when the critical angle of attack of the airfoil (cross-sectional shape of the wing) is exceeded. However, there is also an airspeed (speed of the bird relative to the wind) limit value below which the lift is insufficient to support the bird weight. This is explained by the proportional relation between lift and airflow velocity (lift is proportional to the square of the airflow velocity). Therefore, the estimation of airspeed is also a good indicator of imminent stall. [7]

How could we determine the airspeed ? In flight, the airfoil produces small vortices that come off from the upper and lower surfaces of the trailing edge (rear part of the wings with respect to the airflow), this produces vibrations along the trailing edge. There is a relation between the frequency of formation and shedding of the vortices (causing the vibrations) and the velocity of the airflow. [25] Thus, we could make the assumption that detecting the frequency of vibrations on the trailing edge would permit to determine airspeed. Therefore, the mechanoreceptors located on the filoplumes attached to the secondary flight feathers (which can be approximated as the trailing edge) are relevant to study.

If we consider flight optimisation, airspeed is related to the required aerodynamic power that the bird has to provide in order to generate a sufficient lift force to fly. This relation can be represented by an U-shaped curve. The range of efficient speeds in flight which minimises the energy cost per distance travelled is very narrow and very important to adopt for migratory birds. Thus, optimisation of energy cost requires airspeed information. [7] In addition, it has been demonstrated that the most efficient flapping frequency and flapping amplitude are closely related to airspeed. [26] This validates the choice of airspeed as relevant parameter to study, even if we will more focus on flight stability than on flight optimisation.

It would be too complex to model all the sensory system, so we limit our model by considering only the mechanoreceptors located within the supporting tissues of the alula joint and in the covert feathers of the dorsal wing (responsible for detecting elevation of feathers, that is stall onset when the elevation is sufficiently important).

# 3 Problem statement

The stall phenomenon is the most important risk to which any natural (birds, bats, insects) or artificial (aircraft, helicopters, drones) flying body is subject. Stall is a loss of lift that results in a drop in altitude. The objective of this master thesis is to design a controller to stabilise a bird model undergoing stall in flight. This bird model was made by Gianmarco Ducci, PhD student at the Ecole Polytechnique de Louvain, and will be presented in more detail in the description of the bird model chapter.

The controller represents the bird reactions to stall onset. Given that accurate geometric data about bird flight currently do not exist in scientific literature and are quite difficult to obtain experimentally, the reactions implemented in the controller are based on realistic assumptions that could not be verified with certainty. This is one of the main limits of the model.

The detection of stall onset is assumed to be carried out by the mechanoreceptors located within the supporting tissues of the alula joint and in the covert feathers of the dorsal wing. Indeed, these sensory receptors are assumed to sense vibrations due to turbulence which give an indirect measurement of the mean angle of attack. This indirect measurement is assumed to be compared to the critical angle of attack (corresponding to the stall threshold) which is assumed to be known by the bird from experience or instinct. If the integrating centre interprets from the sensory signal that stall is occurring, the bird should adjust its flight parameters to avoid stall. The reactions of the bird are represented by the presence of the controller in our system.

The objective of this master thesis consists into designing a controller that can avoid stall. This raises several research questions. For which condition(s) should the controller consider that stall is occurring ? Which flight parameter(s) should the bird change to stop stalling ? Which type of controller would be the most relevant to avoid stall ? Which parameter(s) would be the most suitable for this type of controller ? What are the limits of this model ?

# 4 Bird model

## 4.1 General parameters influencing bird flight

The bird is subjected to four forces : lift, drag, thrust and weight. The free body diagram is presented on figure 4.1. In the body frame, lift and weight are perpendicular to the oncoming air, while thrust and drag are parallel to the oncoming air. The lift is opposed to the weight and oriented upwards. The thrust is opposed to the drag and oriented in the direction of bird motion. The bird can be considered as free to rotate in 3 directions : roll (rotation around the front-to-back axis), pitch (rotation around the side-to-side axis) and yaw (rotation around the vertical axis) (see figure 4.1).

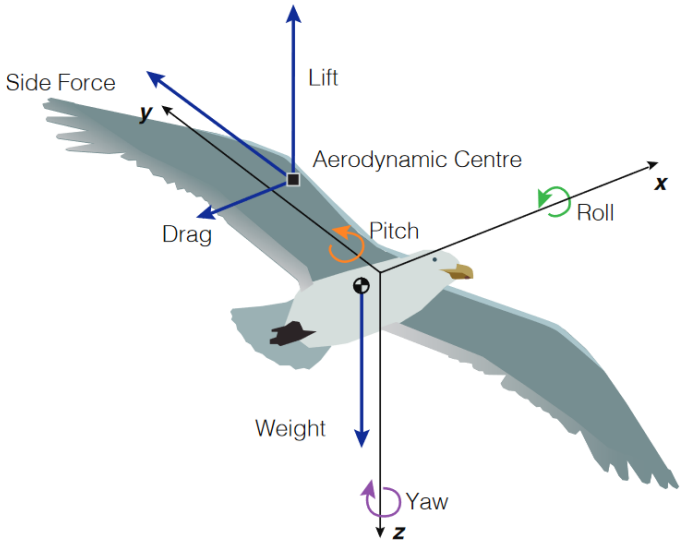


**Figure 4.1:** *Free body diagram of a gliding bird [27]*

The wings of the bird generate most of the aerodynamic forces required for the flight, while the body and the tail are used for flight control, lift enhancement and drag reduction [28].

To measure the total wing velocity during flapping, the body velocity and the relative wing motion should both be taken into account. The magnitude and the orientation of the relative wing motion depends on stroke angle (angle between the wing and the side-to-side axis), spanwise position and angular velocity. [6]

A method for non-intrusive aerodynamic force measurement has been developed for freely flying animals and robots [29]. It consists of using the Navier-Stokes equations in order to study the free flight of the animal or robot in an aerodynamic force platform (AFP). The AFP is a box equipped with loadcells which measure the net unsteady fluid force produced by the animal or the robot in flight. The loadcells work on the principle of the Newton's third law applied on the fluid (to every action there is always opposed an equal reaction).
As velocity, pressure and shear stress can be determined over the complete surface of the AFP, the net fluid force can be integrated exactly, thanks to the Navier-Stokes equations with the AFP as control surface. The measurements indicate that the thrust generation and weight support are mainly provided during the downstroke phase, during take-off and landing. [29]

It has also been shown that [30] the same result is obtained in flight (thrust generation and weight support are also mainly provided during the downstroke phase, in flight).

The aerodynamic forces (lift, drag and thrust) depend partially on wing properties controlled by the bird : surface area exposed to the wind, velocity of wing beats and angles of the wings and of the spreadable feathers with respect to the trajectory. The feathers generally have a stiff leading edge and a flexible trailing edge, to ensure a better robustness to the wind efforts.

The lift, drag and thrust forces also depend on properties of the wing that can not be controlled by the bird such as wing (active or passive) morphing and wing robustness. These forces also depend on properties of the environment : air density that varies with altitude and incident velocity. The coefficients of lift, drag and thrust depend mainly on the ratio of inertial forces versus viscous forces. [6]

In terms of flight control, the primary mechanisms which drive the modulation of aerodynamic forces are the wing velocity on the shoulder, the wing shape and angle of attack of the bird. Wing velocity is proportional to wing length multiplied by wing angular velocity, thus some of these parameters are interdependent. [6]

## 4.2 Description of the bird model

The bird model for which the controller was designed by Gianmarco Ducci, PhD student at the Ecole Polytechnique de Louvain. In this section, the assumptions and the functioning of the model will be explained, before detailing the functioning of the controller which will be presented in the next section. These explanations are based on the paper [31] and on the Python code of the bird model which is available at the address [2].

### 4.2.1 Hypotheses of the bird model

The bird model makes the simplifying assumption that the bird's kinematics are imposed, which means that the bird's wing flapping is not influenced by air resistance or aerodynamic turbulence. This is equivalent to consider that the bird is in a wind tunnel and that there are no dynamics as the bird is not considered to be moving. It is also assumed that all aerodynamic forces act on the wings and not on the main body.

This model is mainly based on large scale and fast migratory birds. This type of bird has the characteristic of having wings whose mass is much lower than the mass of their body. It is therefore possible to neglect the effect of wing beats on the displacement of the centre of gravity. Thus, we can assume that the inertia effect of the wings on the main body can be neglected. The large scale size of the wings of this type of bird also allows us to use a quasi-steady-state approximation for the dynamic model.

The geometric model of the bird does not have a tail. As a reminder, the tail of a bird allows to generate lift, to control drag and to facilitate direction changes. Indeed, the aerodynamic effects of the tail are modelled indirectly by sweeping the wings around the centre of mass. This sweep of the wings around the centre of mass allows the generation of nose-up and nose-down pitching moments.

To simplify, the flight of the bird is considered only in the longitudinal plane (plane of symmetry of the bird). Thus, it is considered that the bird has only 3 degrees of freedom (2 in translation, 1 in rotation). In addition, the lateral forces, roll moments and yaw moments are equal to zero because of this plane of symmetry and are therefore not considered by the model. It is assumed that the kinematics of the left and right wings of the bird are symmetrical.

### 4.2.2 Functioning of the bird model

#### 4.2.2.1 Longitudinal motion

The modelled bird is considered as a rigid body located at its centre of mass. We assume that the bird is in a wind tunnel, so we can consider a fixed reference frame. We choose a reference frame that takes the bird's centre of mass as its origin. The x-axis is defined in the longitudinal direction of the wings (considering that the wings are in an extended position). The y-axis is defined perpendicular to the back of the bird. The z axis is defined in the direction of the bird's tail (which is neglected in this model). This reference frame is shown in figure 4.2.

As the flight of the bird is only considered along the longitudinal plane, the modelled bird has 3 degrees of freedom: 2 degrees of translation along the x and z axes and 1 degree of rotation along the x axis which corresponds to the pitch angle $\theta$.

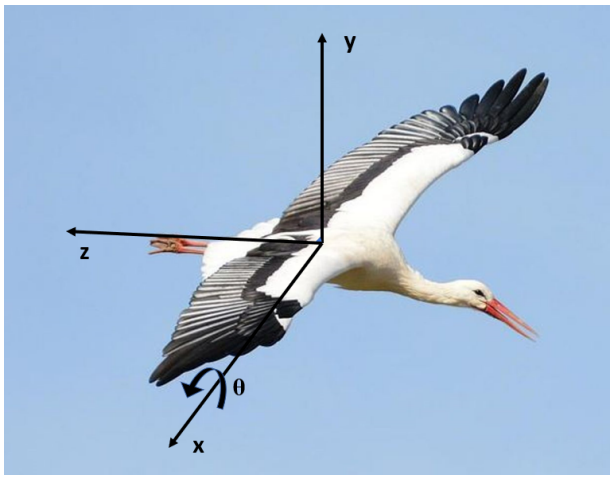


**Figure 4.2:** *Reference frame for the bird model [32]*

The model uses the conventional form of the Newton-Euler equations for a fixed wing aircraft:

$$\dot{u} = -qw - gsin(\theta) + \frac{1}{m_b} F_z(z(t), t)$$

$$\dot{w} = qu + gcos(\theta) + \frac{1}{m_b} F_y(z(t), t)$$

$$\dot{q} = \frac{1}{I_{xx}} M_x(z(t), t)$$

$$\dot{\theta} = q$$

u is the velocity component along the z axis.
w is the velocity component along the y axis.
$\theta$ is the pitch angle describing the body inertial orientation.
q is the body angular velocity ($\theta$ derivative).
t is the time.
g is the gravitational acceleration. $m_b$ is the bird mass.
$I_{xx}$ is the moment of inertia around the x axis.
$F_z$ and $F_y$ are the aerodynamic loads acting on the bird. $M_x$ is the pitching moment.
The state vector describing the longitudinal motion is given by $z = \{u, w, q, \theta\}$.

#### 4.2.2.2 Wing kinematics

The kinematic model of the bird assumes that the bird is a rigid body consisting of a main body and two wings. Each wing consists of three rigid bodies: the arm, the forearm and the hand. Wing morphing is achieved by relative movements between these wing sections.

The bird's plumage is represented by master feathers attached to the wing segments (arm, forearm, hand). Each main feather is attached to one of these wing segments by two rotational degrees of freedom allowing spreading and pitching, except for the one furthest from the bird's body which is aligned with the last bone segment. Feather movements are constrained by kinematic relationships that depend on the angles between the wing segments. This permits to make them spreading and folding smoothly with the wing. The kinematic model of the bird wing is represented on figure 4.3.

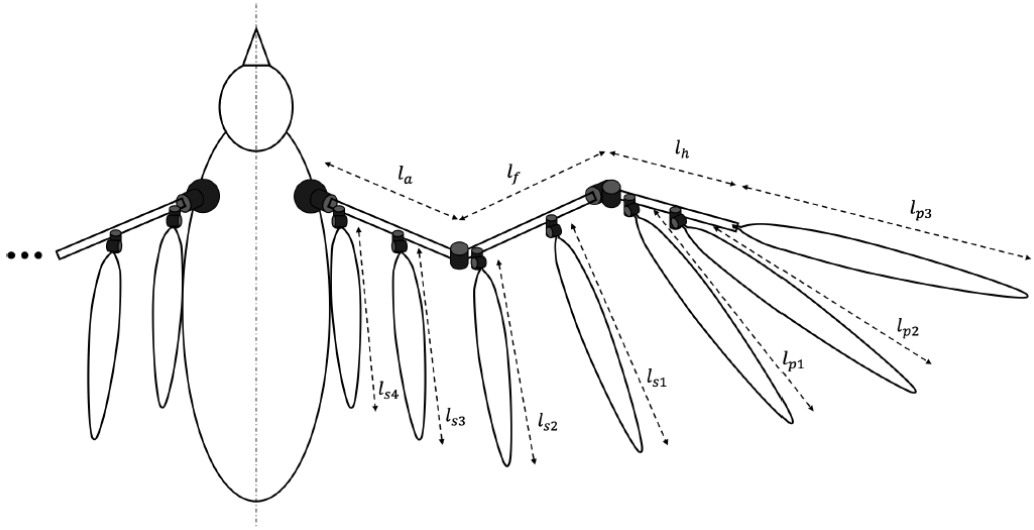


**Figure 4.3:** *Top view of the bird wing kinematic model [31]*

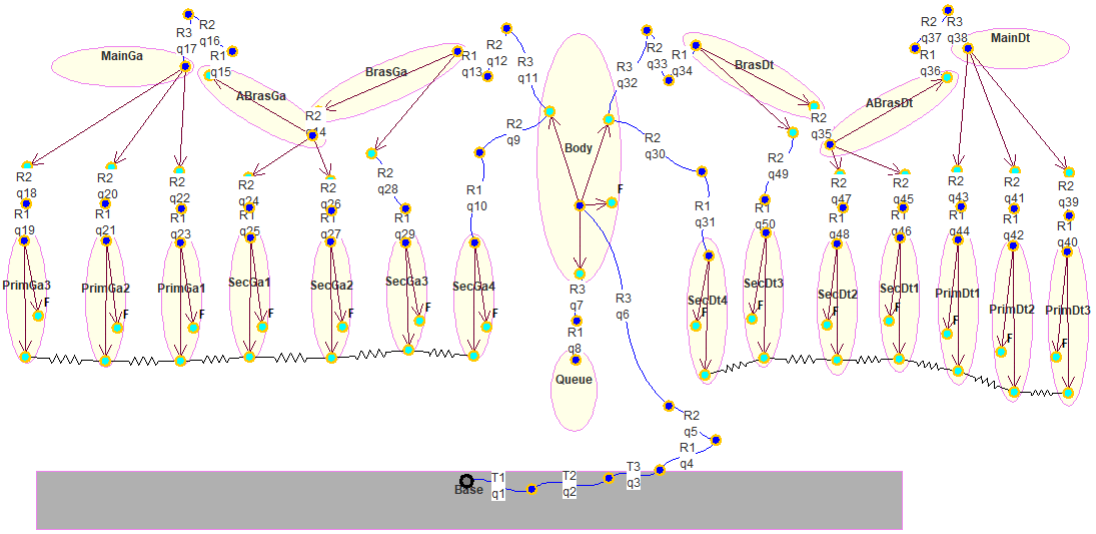


**Figure 4.4:** *Kinematic model of the bird designed by Victor Colognesi, PhD student at Ecole Polytechnique de Louvain, with the Robotran software developed by the MEED which is part of the Institute of Mechanical, Material and Civil engineering of the Université Catholique de Louvain*

The kinematic model of the bird has been designed by Victor Colognesi (4.4), PhD student at Ecole Polytechnique de Louvain. It is important to notice that this model uses the hypothesis that the elbow has one degree of freedom (along the y axis) instead of two (along the x and y axes) in the model considered for this master thesis and that the wrist has two degrees of freedom in this model (along the x and y axes) instead of one (along the y axis) in the model considered for this master thesis. In other words, the degree of freedom along the x axis for the wrist in Victor Colognesi model is replaced by the degree of freedom along the x axis for the elbow in the model considered for this master thesis. This does not make any significant change, this is why this model has been used in order to better visualise the changes in the bird geometry in flight.

The bird model was inspired by large-scale flapping fliers, in particular by the northern bald ibis (Geronticus eremita). Indeed, the bird model took the dimensions of the bones and feathers of the northern bald ibis. This bird was chosen for the high aspect ratio of its wing and for its non-stop flapping flight. The aspect ratio of a wing is the ratio of its span to its mean chord, that is the square of the wingspan divided by the wing area.

We consider the frame shown in figure 4.2 as the reference frame for all the joints of the bird. It is assumed that the shoulder has 3 degrees of freedom along the x, y and z axes, that the elbow has 2 degrees of freedom along the x and y axes, and that the wrist has only one degree of freedom along the y axis.

Each joint angle (noted i) is assumed to follow a harmonic trajectory $q_i(t)$ given by the following formula:

$$q_i(t) = q_{0,i} + A_i sin(\omega t + \phi_{0,i}) \tag{4.1}$$

$A_i$ is the amplitude of the periodic trajectory $q_i(t)$ of the joint angle. This corresponds to the difference between the maximum angle and the minimum angle taken by the joint. This angle is defined along a certain axis of rotation. In other words, $A_i$ is the flapping amplitude of the joint angle along a certain direction.

$\phi_i$ is the phase of the periodic trajectory of the joint. This corresponds to the angle that the joint takes at the initial time $t = 0$. In other words, $\phi_i$ is the shift of the periodic trajectory pattern along the time axis.

$q_{0,i}$ is the horizontal offset of the periodic trajectory of the joint. This represents the average value of the angle that the joint takes. In other words, $q_{0,i}$ is the offset of the periodic trajectory pattern along the angular axis.

$\omega = 2\pi f$ is the pulsation of the wing beats. f is the frequency of the wing beats, which is identical for each joint.

Given that the kinematics is assumed to be symmetrical and taking into account the assumptions on the number of degrees of freedom of each joint, 19 parameters allow to determine a particular set of wing kinematics. These 19 parameters are the amplitude, phase and offset of the periodic trajectory of the shoulder angle along the x, y and z axes; the amplitude, offset and phase of the periodic trajectory of the elbow angle along the x and y axes; the amplitude, offset and phase of the periodic trajectory of the wrist along the y axis; and f, which is the frequency of the wing beats.

Therefore, the bird model is a 4 states non autonomous system for which the aerodynamic terms depend on the current state vector describing the longitudinal motion ($z = \{u, w, q, \theta\}$) and of the instantaneous configuration of the wing which is determined by the 19 parameters given in the above paragraph.

#### 4.2.2.3 Aerodynamic model

Using the assumption of quasi-stationary flight for large scale birds, the aerodynamic model uses a quasi-stationary lifting line approach. The wake is assimilated to straight and infinitely long vortex filaments at each time step of the simulation. The aerodynamic forces acting on the wing are applied to the discretised points of the lifting line (drawn in red on figure 4.4) which follows the wing span.

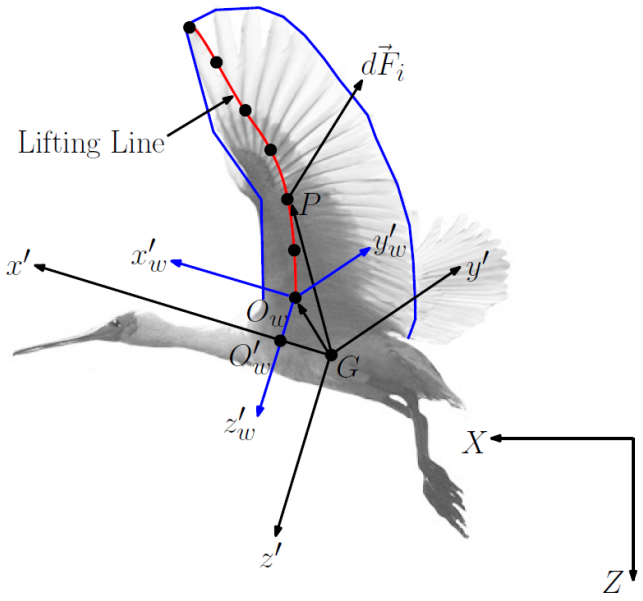


**Figure 4.5:** *Discretisation of the lifting line [31]*

The lifting line can be defined as the line passing through the quarter of the chord. The chord is the imaginary line between the leading edge (front part of the airfoil facing the flow) and the trailing edge of an airfoil (rear part of the airfoil with respect to the flow direction).

In the case of the bird model, the leading edge is defined as passing in a straight line from the shoulder to the wrist and then to the tip of the feather which is the furthest from the main body. The trailing edge is defined as connecting the end of each feather from the innermost to the outermost. The lifting line is then obtained by iterations, to ensure that it is located at the distance of one quarter of the chord and that it is orthogonal to the chord at each point.

The lifting line equation used by the model for the reference frame of figure 4.2 is given by :

$$\Gamma(\mathbf{x}) = \frac{1}{2}c(\mathbf{x})C_{l,\alpha}\left[||\mathbf{U}||\alpha(\mathbf{x}) - \frac{1}{4\pi}\sum_i \left( - d\Gamma_i \frac{(\mathbf{x}-\mathbf{x_i})\times\hat{\mathbf{e}}_\mathbf{z}}{||\mathbf{x}-\mathbf{x_i}||^2}\right)\cdot\hat{\mathbf{e}}_\mathbf{n}\right]$$

i is the index for discretised elements of the lifting line.
$\Gamma(\mathbf{x})$ is the circulation of the lifting line.

$c(\mathbf{x})$ is the local aerodynamic chord length.
$\alpha(\mathbf{x})$ is the local angle of attack.
$||\mathbf{U}||$ is the norm of the relative velocity seen by the wing profile. $\mathbf{U} = \mathbf{U}_\infty - \mathbf{U_{kin}}$ with $\mathbf{U}_\infty$ which is the flight speed and $\mathbf{U_{kin}}$ which is the wing motion.
$C_{l,\alpha}$ is the slope of the lift curve.
$d\Gamma_i$ is the circulation of a vortex tube.
$\hat{\mathbf{e}}_\mathbf{n}$ is the unit vector which is orthogonal to the plane containing the lifting line.

The demonstration of the lifting line equation is given in the paper [31].

Finally, the aerodynamic force acting on each discretised point of the lifting line can be computed and we obtain the corresponding contributions for each axis :

$$F_z = \sum_{i=1}^{N} (\mathbf{dF_i}) \cdot \hat{\mathbf{e}}_\mathbf{z}$$

$$F_y = \sum_{i=1}^{N} (\mathbf{dF_i}) \cdot \hat{\mathbf{e}}_\mathbf{y}$$

The pitching moment is given by:

$$M_x = \sum_{i=1}^{N} (\mathbf{G} \cdot \mathbf{P_i}) \times (\mathbf{dF_i}) \cdot \hat{\mathbf{e}}_\mathbf{x}$$

$F_z$ is the component along the z axis of the aerodynamic force acting on the bird.
$F_y$ is the component along the y axis of the aerodynamic force acting on the bird.
$M_x$ is the pitching moment around the x axis acting on the bird.
$\mathbf{G}$ is the position vector of the bird centre of mass.
$\mathbf{P_i}$ is the position vector of the i-th discretised point of the lifting line.

# 5 Description of the designed controller

## 5.1 The design steps of the controller

The objective of the controller is to stabilise the flight of the bird model (presented in the previous chapter) by stopping the stall onset when it is detected. Thus, the principle of the controller is to give instructions to the bird to change the parameters of its wing kinematics when stall is detected.

Stall can be defined as a sudden reduction of the lift occurring when the angle of attack of the bird reaches or exceeds the critical angle of attack. A common approximation of the critical angle of attack is 15°. Thus, we choose 15° as the threshold for stall occurrence. Mathematically, the critical angle of attack corresponds to the maximisation of the lift coefficient. Physically, it corresponds to the stall angle of attack beyond which the airflow begins to separate from the upper surface of the airfoil.

Below the critical angle of attack, the lift coefficient increases with the angle of attack. Beyond the critical angle of attack, the lift coefficient decreases if the angle of attack keeps increasing. When the critical angle of attack is reached, only decreasing the angle of attack does not permit to avoid stall, because the angle of attack increases in order to increase the lift coefficient (that is necessary to provide enough lift to compensate the bird's weight). A high angle of attack can be necessary in case of low bird speeds for which the lift produced by the wings is lower than for high speed flights. Indeed, the smaller the speed of the flyer is, the greater the angle of attack is needed to produce lift equal to the flyer's weight.

The first step in designing the controller is to define under which conditions the bird is subjected to the aerodynamic stall phenomenon. The second step is to define which flight parameters need to be changed for the bird to stop stalling. The third step is to define which type of controller would be the most suitable to induce a type of response that would allow the bird to quickly exit the stall. The fourth step is to determine the most suitable parameters for this type of controller (this will use the Results chapter, as this choice of parameters is based on empirical data).

### 5.1.1 Condition for which the bird is subjected to stall

We have already chosen to set the threshold for the critical angle of attack at 15°. Thanks to the mechanoreceptors located within the supporting tissues of the alula joint and in the covert

feathers of the dorsal wing (responsible for detecting the elevation of feathers, that is stall onset when the elevation is sufficiently important), the bird can have an indirect idea of the value of the angle of attack. In the simulation, the majority of the calculations are performed by using the discretised points of the lifting line as application points. The angle of attack values are also evaluated at these points.

The angle of attack for the i-th chord section is computed as follows (this formula can be deduced geometrically from figure 5.1):

$$\alpha_i = arctan\left(\frac{\mathbf{d_v} \cdot \mathbf{n}}{\mathbf{d_v} \cdot \mathbf{d_c}}\right)$$

$\mathbf{d_v}$ is the direction of the relative velocity seen by the chord section.
$\mathbf{n}$ is the normal to the chord section.
$\mathbf{d_c}$ is the direction of the chord line.

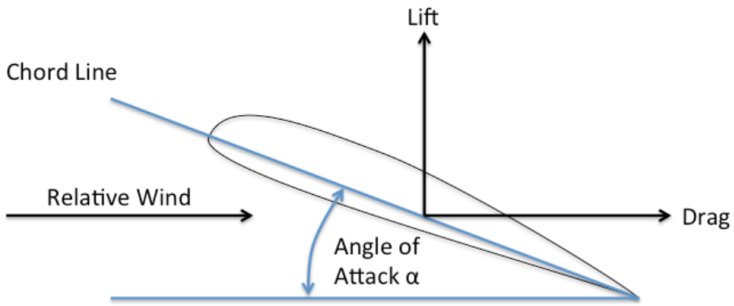


**Figure 5.1:** *Graphical representation of the angle of attack of the wing chord section [33]*

The stall threshold (which is the value of the critical angle of attack) is defined for a general value of the angle of attack over the entire chord line. In order to obtain this general value of the angle of attack, it was decided to take a weighted average of the angle of attack for which the weights are the lengths of the chord sections. Indeed, if stall occurs in sections with a small chord length (such as wing tips), the influence of stall is much weaker than if stall occurs in sections with a large chord length (such as towards the bird body) for which being affected by stall would be much more problematic. However, there is an exception for the chord sections which are the closest to the bird shoulders, because they are affected by the shoulder movements in flight.

Thus we define that the bird is considered to be subjected to stall if the value of the angle of attack averaged over the chord length of each chord section exceeds the threshold for stall occurence (that is 15°).

### 5.1.2 Flight parameters that need to be changed for the bird to stop stalling

For a better graphical representation, the figure 5.2 illustrates the wing kinematics over one flapping cycle. For each position at time t, the red line corresponds to the lifting line (where the aerodynamic forces are computed), the green lines correspond to the leading edge (for the green line facing the air flow) and to the trailing edge (for the green line at the rear) and the blue lines correspond to the arm, the forearm, the hand and the 7 master feathers.

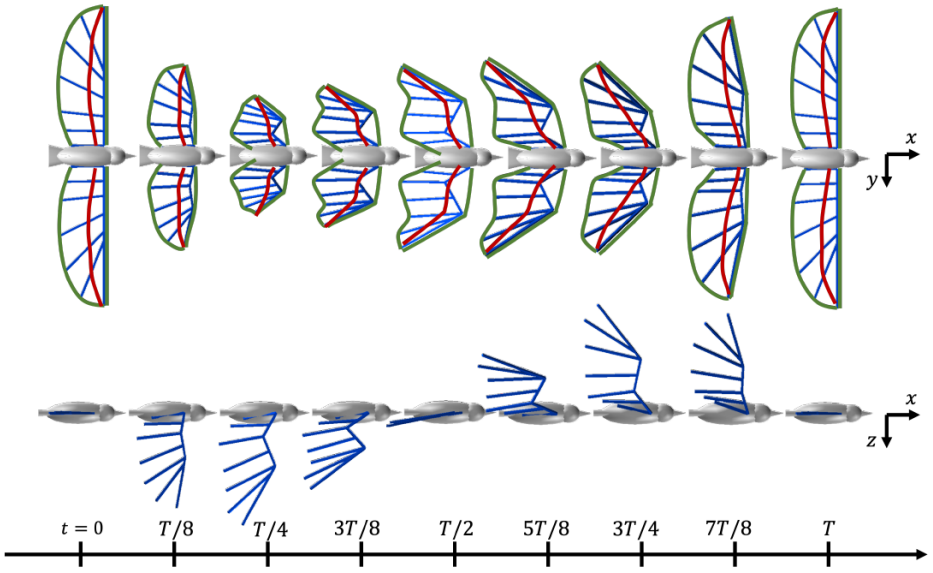


**Figure 5.2:** *Snapshots of the wing kinematics over a flapping cycle [31]*

The parameters of the shoulders directly influence the angle of attack of the bird, as they are at the origin of the orientation of the arms (bone segment between the shoulder and the elbow) and thus of the orientation of the wings. Geometrically, we can easily see that the two parameters affecting the most the angle of attack are the shoulder offset along the x axis and the elbow offset along the x axis (defined as the longitudinal direction of the wings, see figure 4.2).

As a reminder, the offset corresponds to the horizontal offset of the periodic trajectory of the joint, that is the average value of the angle that the joint takes. Thus, it is the $q_{0,i}$ term from the equation 4.1 reminded below:

$$q_i(t) = q_{0,i} + A_i sin(\omega t + \phi_{0,i})$$

The reaction of the bird to avoid stall should be to twist down its wing along the x axis, which means to decrease the offset of its joints along the x axis. We will only decrease the offsets of the harmonic trajectory of the shoulder and of the elbow, because we assume that the wrist does not have a degree of freedom along the x axis and it is not very important if stall affects the wing tips (because of the small chord section), as explained in the previous subsection.

There are no accurate studies on bird morphologies. How birds move their wings in flight is not known with accuracy. Thus, some joint angles in the simulation might be unrealistic.

### 5.1.3 Choice of the type of controller

The inputs of the biomechanical model are the relative velocity seen by the wing profile and the initial prescribed kinematics. The initial prescribed kinematics are the flapping frequency, the offsets, amplitudes and phases of the shoulder along the x axis, along the y axis and along the z axis, the offsets, amplitudes and phases of the elbow along the x axis and along the y axis, and the offset, amplitude and phase of the wrist along the y axis. The reference frame is still the one defined on figure 4.2.

The sensory receptors convert the vibrations of the alula and of the dorsal wing covert feathers into an indirect measurement of the angle of attack. If this indirect measurement of the angle of attack exceeds the critical angle of attack (that is the threshold of 15°), the controller provides feedback by sending the instructions to decrease the offset of the harmonic trajectory of the shoulder joint angle along the x axis and to decrease the offset of the harmonic trajectory of the elbow joint along the x axis. The block diagram of the controller is represented on figure 5.3.

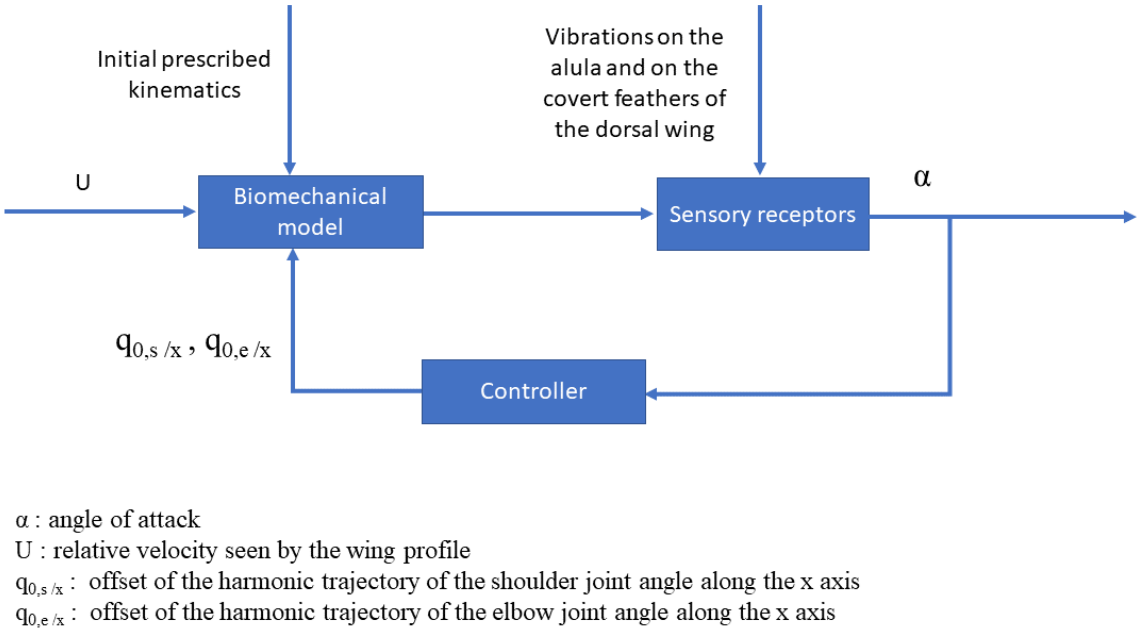


**Figure 5.3:** *Block diagram of the controller*

The first design idea for the controller was to implement a proportional controller. However, the bird simulation sometimes shows aberrant values at some singular points of the computation. These singular points are not representative of the reality. An instantaneous response which does not take into account the past values (that is characteristic of a proportional controller) implies a risk of instability if a value of the angle of attack much higher than the 15° threshold is detected because of a singular value of the simulation. Therefore, a proportional controller did not seem appropriate in our case.

An integral controller was chosen in order to take into account the sum of the error over time to adapt its feedback. The "error" is defined as the entry level in the stall region (that is the difference between the current angle of attack and the 15° threshold). Thus, the current and past values of the angle of attack are taken into account for the current feedback. We chose to multiply the integral gain by the entry level in the stall region, in order to have a more important answer from the bird (that is a decrease of the shoulder and elbow offsets) if the angle of attack exceeds by far the critical angle of attack. The major disadvantage of an integral controller can be its slow response time. According to the results presented in the next chapter, the integral controller reacts quite fast, but the angle of attack periodically stays dangerously close to the critical angle of attack value for integral gains inferior to 0.9. This will be further developed in the Discussion chapter.

### 5.1.4 Choice of the controller gain

If we consider the results presented in the next chapter, we observe that the angle of attack periodically stays dangerously close to the critical angle of attack value for integral gains inferior to 0.9. The risk of an integral controller with a too high integral gain is to generate a significant oscillation leading to instability. Therefore, the most suitable integral gain in our case is the lower integral gain which is not submitted to the phenomenon of being periodically close to the critical angle of attack value. The choice of its value will be further discussed in the Discussion chapter.

## 5.2 Implementation of the controller

```
# Mean angle of attack taking into account the chord length of each chord
    section:
for j in range(len(angle_of_attack[i])):
  mean_angle_of_attack[i] += angle_of_attack[i][j] * chord[j]
  sum_chord += chord[j]
mean_angle_of_attack[i] /= sum_chord

if (mean_angle_of_attack[i]*180/np.pi) >= stall: # If stall occurs:

  # The controller reduces the shoulder and elbow offsets proportionally
  # to the entrance level in the stall area:
  entrance_level_stall_area = mean_angle_of_attack[i] - stall*np.pi/180
  delta_shoulder_offset_x = -K_i * entrance_level_stall_area
  shoulder_offset_x += delta_shoulder_offset_x
  delta_elbow_offset_x = -K_i * entrance_level_stall_area
  elbow_offset_x += delta_elbow_offset_x

  # New shoulder and elbow objects are created in order to modify the current
  # shoulder and elbow parameters:
  bird_shoulder = Shoulder(axis_x=Joint(shoulder_offset_x, shoulder_amplitude_x,
     shoulder_phase_x), axis_y=Joint(shoulder_offset_y, shoulder_amplitude_y,
    shoulder_phase_y), axis_z=Joint(shoulder_offset_z, shoulder_amplitude_z,
    shoulder_phase_z))
  bird_elbow = Elbow(axis_x=Joint(elbow_offset_x, elbow_amplitude_x,
    elbow_phase_x), axis_y=Joint(elbow_offset_y, elbow_amplitude_y,
    elbow_phase_y))
  mybird.shoulder = bird_shoulder
  mybird.elbow = bird_elbow
```

As a reminder, the bird model has 4 steps:
1) The bird kinematics is imposed.
2) The envelope of the wing is traced based on the morphology of the wing.
3) The lifting lines are extracted based on the envelope.
4) The values of the forces are extracted from the lifting lines.

The controller has 3 steps:
1) The weighted average of the angle of attack (where the weights are the chord length of each chord section) is computed.
2) The offset of the harmonic trajectory of the shoulder joint along the x axis and the offset of the harmonic trajectory of the elbow joint along the x axis are decreased by the product between the integral gain and the entrance level in the stall area.
3) The shoulder and elbow objects are created again in order to change their parameters in the simulation.

We can see that the controller implemented is an integral controller because the "error" (that is the entrance level in the stall region) is multiplied by an integral gain and their product is subtracted to the current values of the shoulder and elbow offsets which are equal to their values at the previous time step, thus the previous correction of the offsets is taken into account in the current correction.

# 6 Results

## 6.1 Angle of attack as a function of the wing chord section position

The figures 6.1, 6.2, 6.3 and 6.4 from this section represent the angle of attack as a function of the wing chord section position during one flapping period divided into 10 time steps. Each curve represents the angle of attack over the chord length for one time step.
For each figure, the graph on the top corresponds to a situation with an initial low entrance in the stall area (the initial shoulder offset along the x axis is equal to 0.3 radians (approximately 17.2°) and the initial elbow offset along the x axis is equal to 0.1 radians (approximately 5.7°)).
The graph in the middle corresponds to a situation with an initial medium entrance in the stall area (the initial shoulder offset along the x axis is equal to 0.4 radians (approximately 22.9°) and the initial elbow offset along the x axis is equal to 0.2 radians (approximately 11.5°)).
The graph at the bottom corresponds to a situation with an important entrance in the stall area (the shoulder offset along the x axis is equal to 0.5 radians (approximately 28.6°) and the elbow offset along the x axis is equal to 0.3 radians (approximately 17.2°)).

The entrance in the stall area is directly linked to the shoulder and elbow offsets along the x axis, because they directly affect the angle of attack. The figure 6.1 represents the 3 scenarios of entrance in the stall area, without controller. The figure 6.2 represents the 3 same scenarios with an integral controller with a small integral gain equal to 0.3. The figure 6.3 represents the 3 same scenarios in the case of an integral controller with a medium integral gain equal to 0.9. The figure 6.4 represents the 3 same scenarios with an integral controller with a higher integral gain equal to 1.5.

We can deduce from the figure 6.2 that an integral controller with an integral gain of 0.3 does not react sufficiently to avoid stall, as the angle of attack is superior to the threshold of 15° on average, for certain time steps, even when the entrance in the stall area is small. On the figure 6.3, we can see that the only angle of attack curve which is above the threshold of 15° is the initial time step, thus the integral controller with an integral gain of 0.9 enables to avoid stall. We can also notice that the average angle of attack for each time step does not go down below -10° below which the orientation of the wings in flight becomes unrealistic and induces instability. We can observe on the figure 6.4 that the average angle of attack becomes dangerously low for certain time steps, for an integral gain of 1.5.

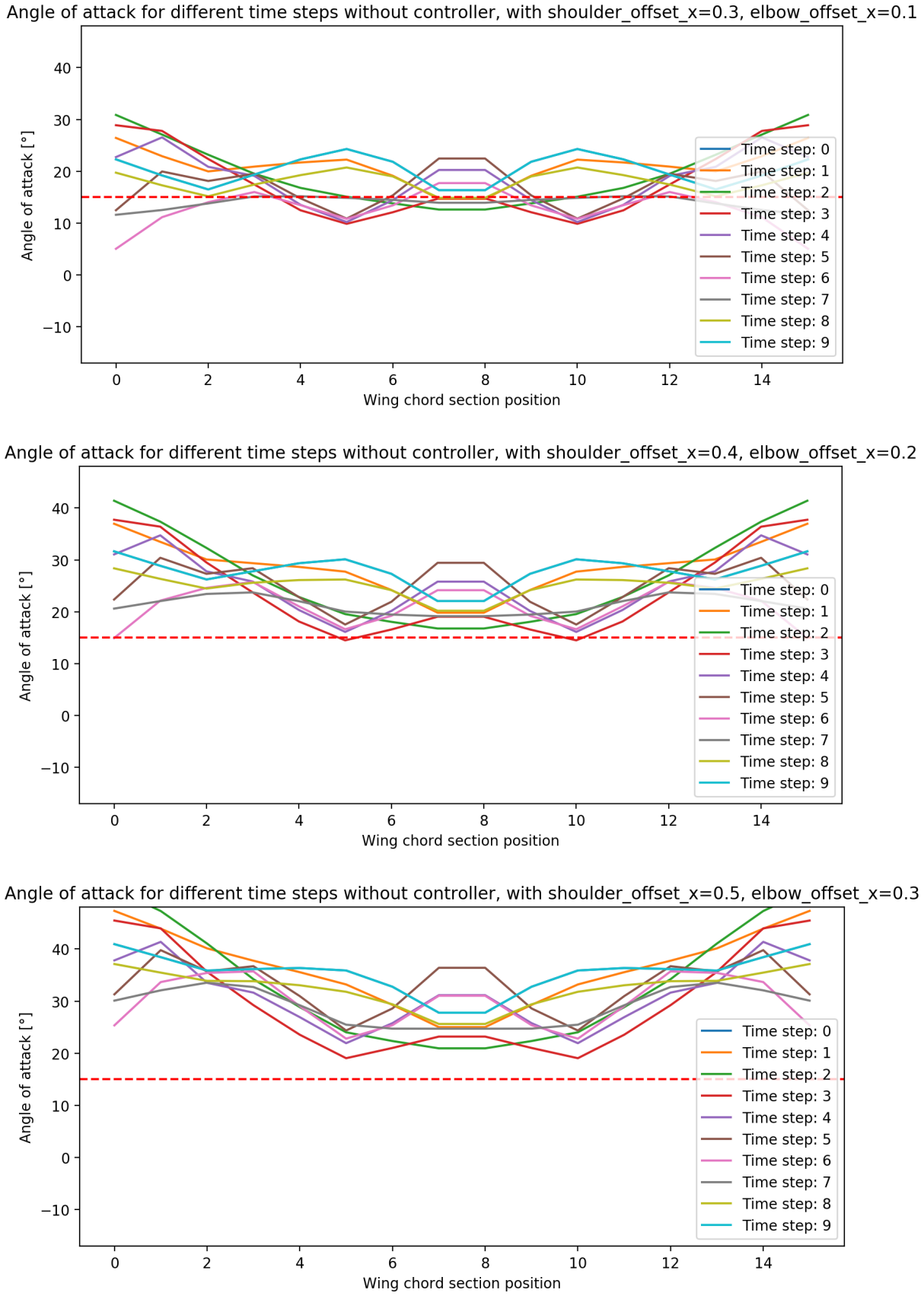


**Figure 6.1:** *Angle of attack as a function of the wing chord section position for different time steps without the controller*

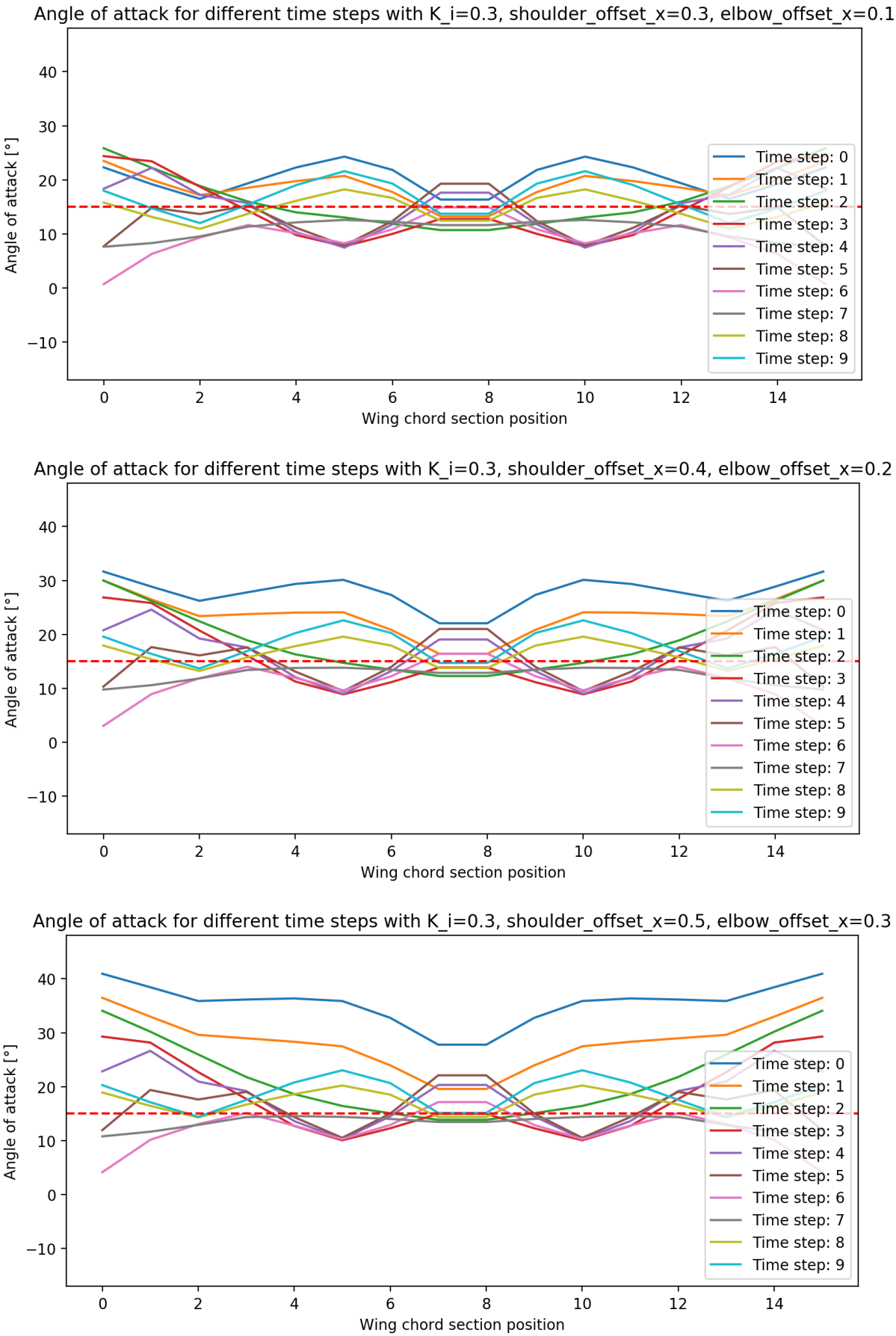


**Figure 6.2:** *Angle of attack as a function of the wing chord section position for different time steps with an integral controller of* $K_i = 0.3$

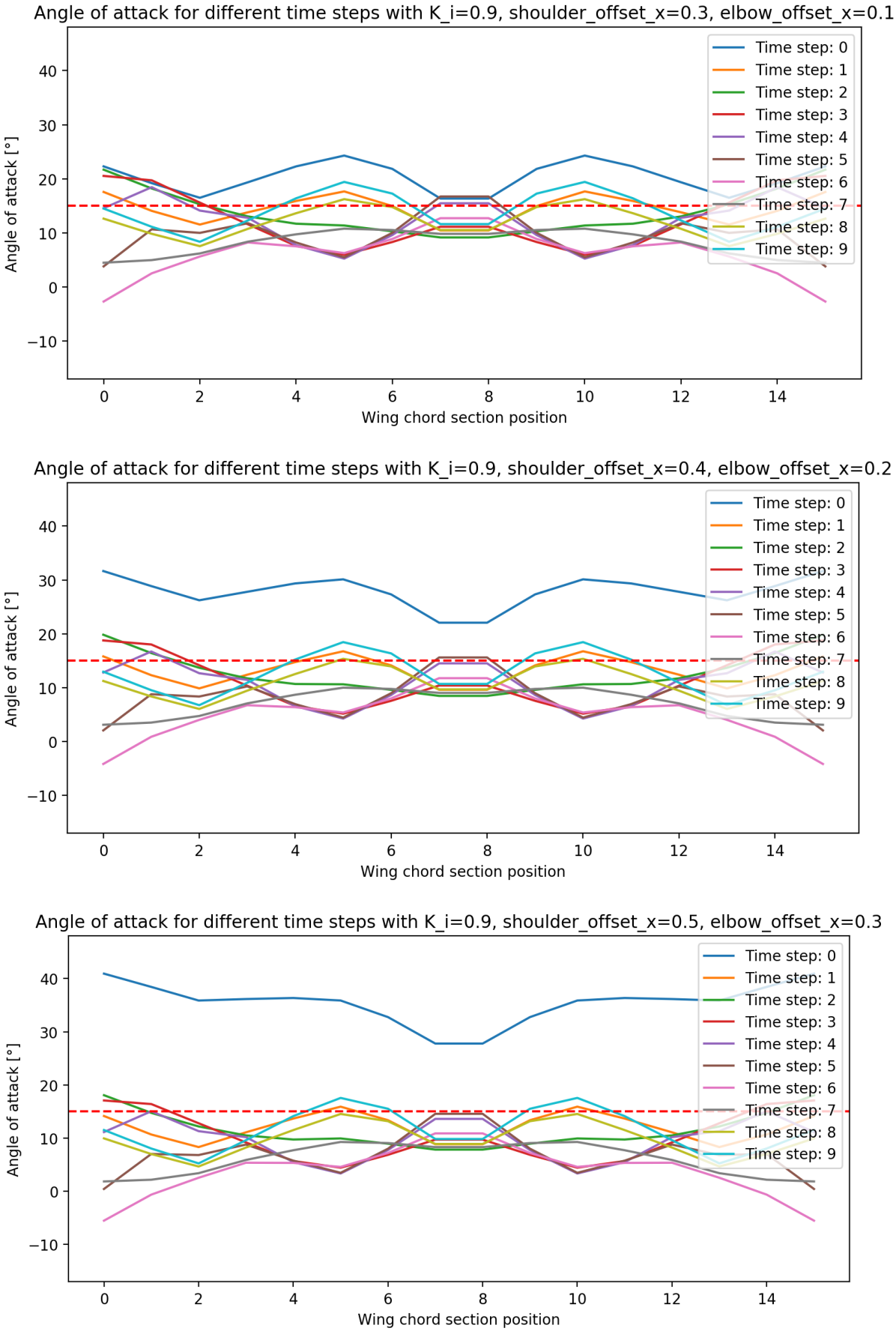


**Figure 6.3:** *Angle of attack as a function of the wing chord section position for different time steps with an integral controller of* $K_i = 0.9$

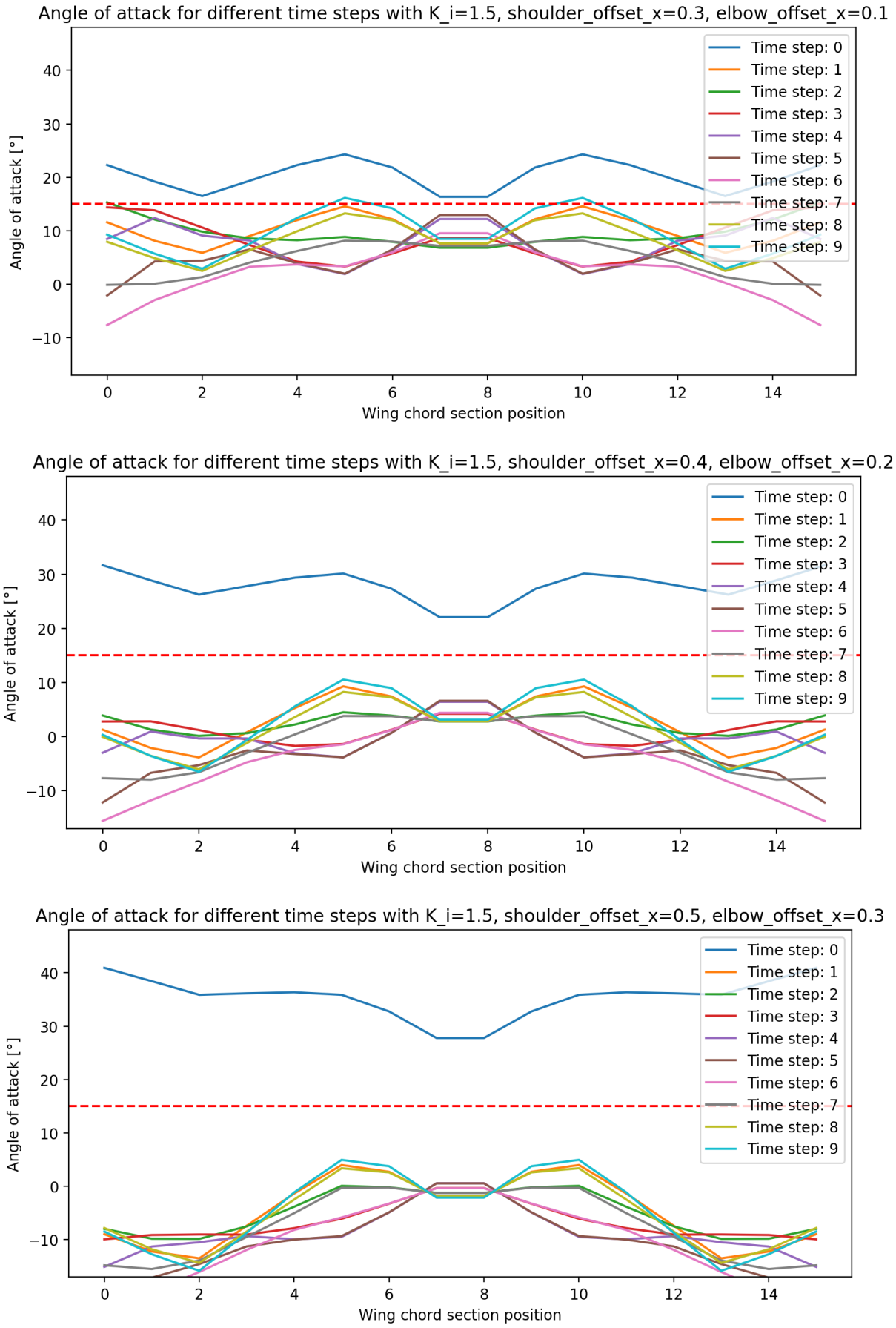


**Figure 6.4:** *Angle of attack as a function of the wing chord section position for different time steps with an integral controller of* $K_i = 1.5$

## 6.2 Mean angle of attack as a function of time

The figures 6.5 and 6.6 from this section represent the mean angle of attack as a function of time for integral gains between 0 and 1.5. An integral gain equal to 0 is equivalent to the absence of a controller. The figure 6.5 represents 3 flapping periods, whereas the figure 6.6 represents 10 flapping periods.
Each figure includes 4 graphs: the upper graph corresponds to a situation with no entrance in the stall area (the shoulder offset along the x axis is equal to 0.2 radians (approximately 11.5°) and the elbow offset along the x axis is equal to 0 radians (0°)).
The graph in second position corresponds to a situation with an initial low entrance in the stall area (the initial shoulder offset along the x axis is equal to 0.3 radians (approximately 17.2°) and the initial elbow offset along the x axis is equal to 0.1 radians (approximately 5.7°)).
The graph in third position corresponds to a situation with an initial medium entrance in the stall area (the initial shoulder offset along the x axis is equal to 0.4 radians (approximately 22.9°) and the initial elbow offset along the x axis is equal to 0.2 radians (approximately 11.5°)).
The graph at the bottom corresponds to a situation with an initial important entrance in the stall area (the initial shoulder offset along the x axis is equal to 0.5 radians (approximately 28.6°) and the initial elbow offset along the x axis is equal to 0.3 radians (approximately 17.2°)).

Given that the joints of the bird model follow the periodic equation 4.1, the bird kinematics is periodic when the controller does not act on the model. This is why the mean angle of attack is periodic for the situation with no entrance in the stall area and when the bird model has stabilised below the 15° stall threshold after the integral controller action.

We can observe on the figures 6.5 and 6.6 that the curves for the integral gains 0.1 and 0.2 take several flapping cycles to almost stabilise. Then, the curves for the integral gains between 0.1 and 0.8 almost merge and become periodically very close to the 15° stall threshold (at the point of the flapping cycle for which the wing is at the upper position). This periodic proximity to the 15° stall threshold may induce instability. It is a default caused by the product between the integral gain and the entrance level in the stall area (see section 5.2).

Nevertheless, this product permits to get a response from the controller which is more quickly adapted to the level of entrance in the stall area. The controller response time can be theoretically calculated by subtracting one flapping period from the time after which the bird performs at least one flapping period that is entirely below the 15° stall threshold. Indeed, the bird kinematics becomes periodic again when the controller is no longer acting on the bird's model (the condition for using the controller is that the average angle of attack is greater than 15°). On the figure 6.5, we can observe that the response time of the controller has the order of magnitude of 100 to 150 ms for the integral gains between 0.9 and 1.5. However, we can see on figure 6.6 that the response time is much more complicated to measure for the integral gains between 0.1 and 0.8 because their angle of attack curves become periodically very close to the stall threshold.

It was initially planned to represent a bar chart of the controller response times for each integral gain, but the bird model simulation present too many singular points to obtain a relevant bar chart. These singular points are due to local problems of extraction of the lifting lines in the bird model simulation, they are not due to the controller. In order to avoid, as much as possible, the impact on the results of these singular values (which are due to the simulation and not to the kinematics of a real bird), the values of the initial shoulder offset and initial elbow offset have sometimes been modified by 0.01 or 0.02, in the inputs of the model for some graphs, in order to have more representative results. These modifications (when there are any) are specified in the titles of the graphs.

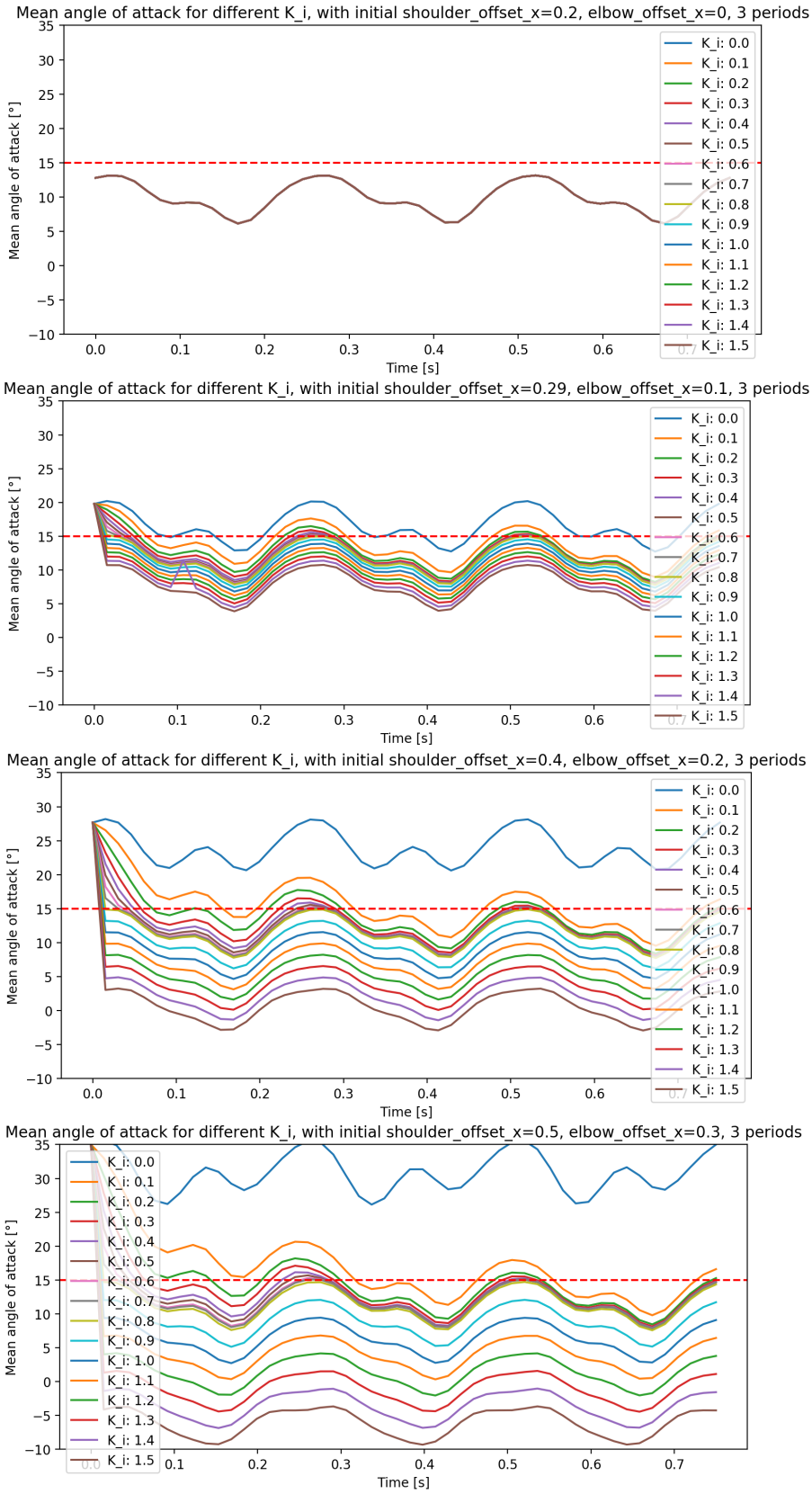


**Figure 6.5:** *Mean angle of attack as a function of time for different integral gains $K_i$ with 3 flapping periods*

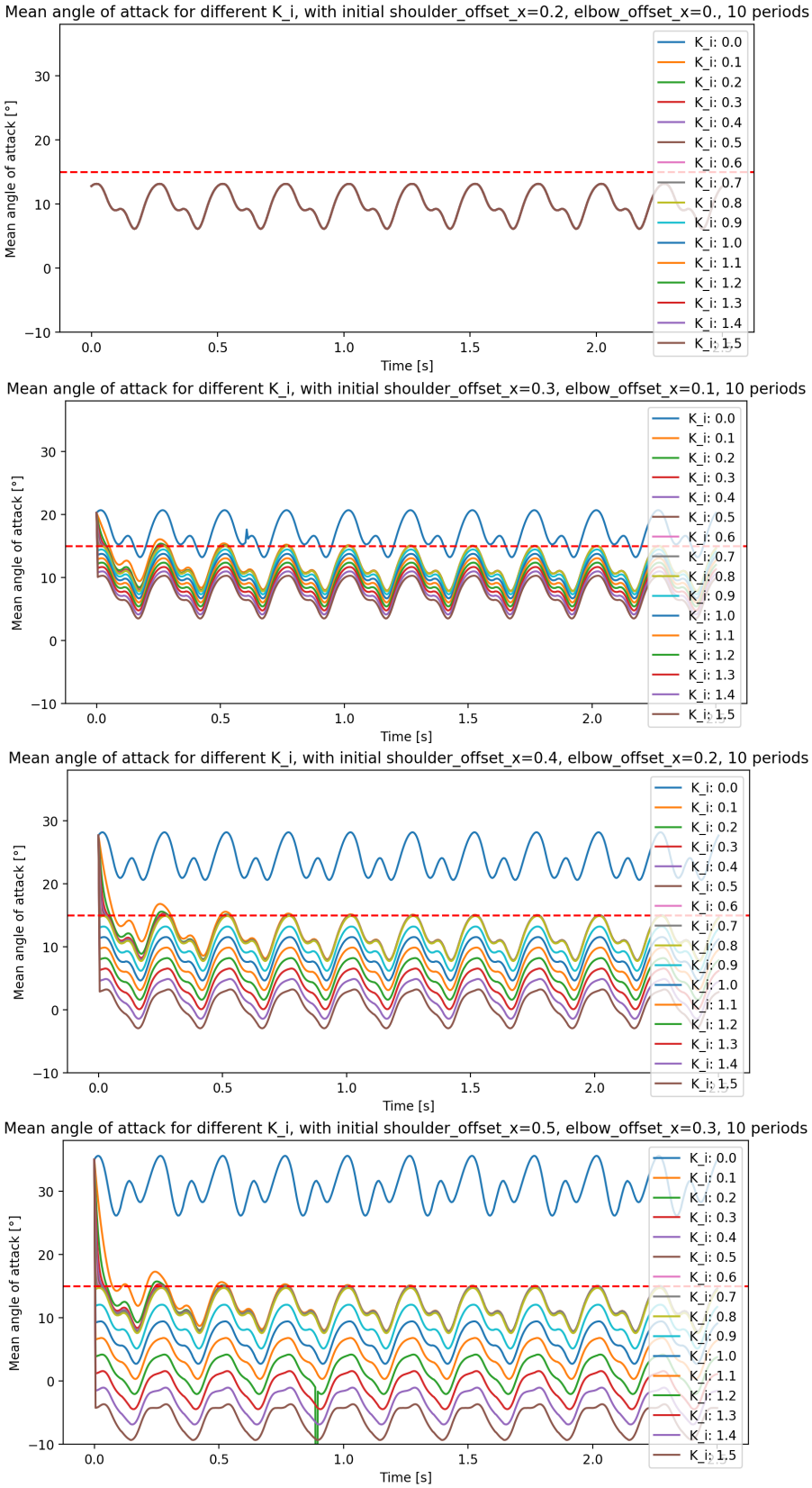


**Figure 6.6:** *Mean angle of attack as a function of time for different integral gains $K_i$ with 10 flapping periods*

## 6.3 Lift and drag as a function of time

The figure 6.8 represents the evolution of lift as a function of time for integral gains between 0 and 1.5, during 3 flapping periods.
The figure 6.9 represents the evolution of drag as a function of time for integral gains between 0 and 1.5, during 3 flapping periods.

Each figure includes 4 graphs: the upper graph corresponds to a situation with no entrance in the stall area (the shoulder offset along the x axis is equal to 0.2 radians (approximately 11.5°) and the elbow offset along the x axis is equal to 0 radians (0°)).
The graph in second position corresponds to a situation with an initial low entrance in the stall area (the initial shoulder offset along the x axis is equal to 0.3 radians (approximately 17.2°) and the initial elbow offset along the x axis is equal to 0.1 radians (approximately 5.7°)).
The graph in third position corresponds to a situation with an initial medium entrance in the stall area (the initial shoulder offset along the x axis is equal to 0.4 radians (approximately 22.9°) and the initial elbow offset along the x axis is equal to 0.2 radians (approximately 11.5°)).
The graph at the bottom corresponds to a situation with an initial important entrance in the stall area (the initial shoulder offset along the x axis is equal to 0.5 radians (approximately 28.6°) and the initial elbow offset along the x axis is equal to 0.3 radians (approximately 17.2°)).

We can deduce the upstroke phase and the downstroke phase, for each flapping period, on the figure 6.8, as the lift increases during the downstroke phase and decreases during the upstroke phase. This is quite intuitive by looking at the figure 6.7 which represents the flapping wing beats of a bird during one flapping period.

We can observe on the figure 6.8 that the greater the integral gain is, the lower the lift will be. Indeed, below the critical angle of attack, the lift coefficient increases with the angle of attack. Thus, if the bird greatly reduces its angle of attack (which is the case for an important reaction to stall onset, that is for an important integral gain), the lift decreases and it may become problematic if the lift is not sufficient to compensate the bird's weight.
We can also observe that for the situation with an important entrance in the stall area (graph at the bottom), the lift curves for integral gains between 1.1 and 1.5 are not sufficient to compensate the bird's weight (which is approximately equal to 11.8 N in the bird model).

We can observe on the figure 6.9 that the greater the integral gain is, the lower the drag will be. Indeed, the drag increases with the angle of attack (as the contact surface and the boundary layer thickness increases if the angle of attack increases), thus a lower angle of attack (due to a more important reaction of the controller) implies a lower drag.

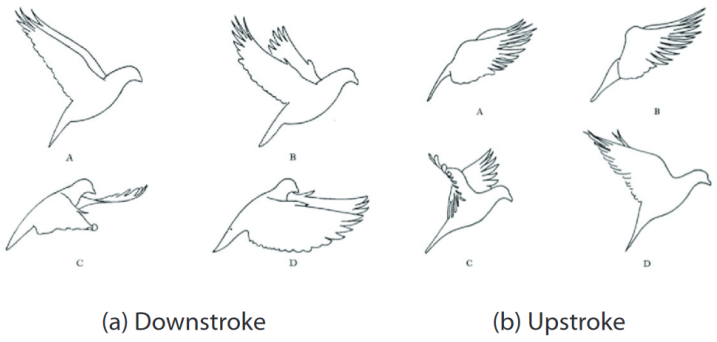


**Figure 6.7:** *Flapping cycle of a pigeon [34]*

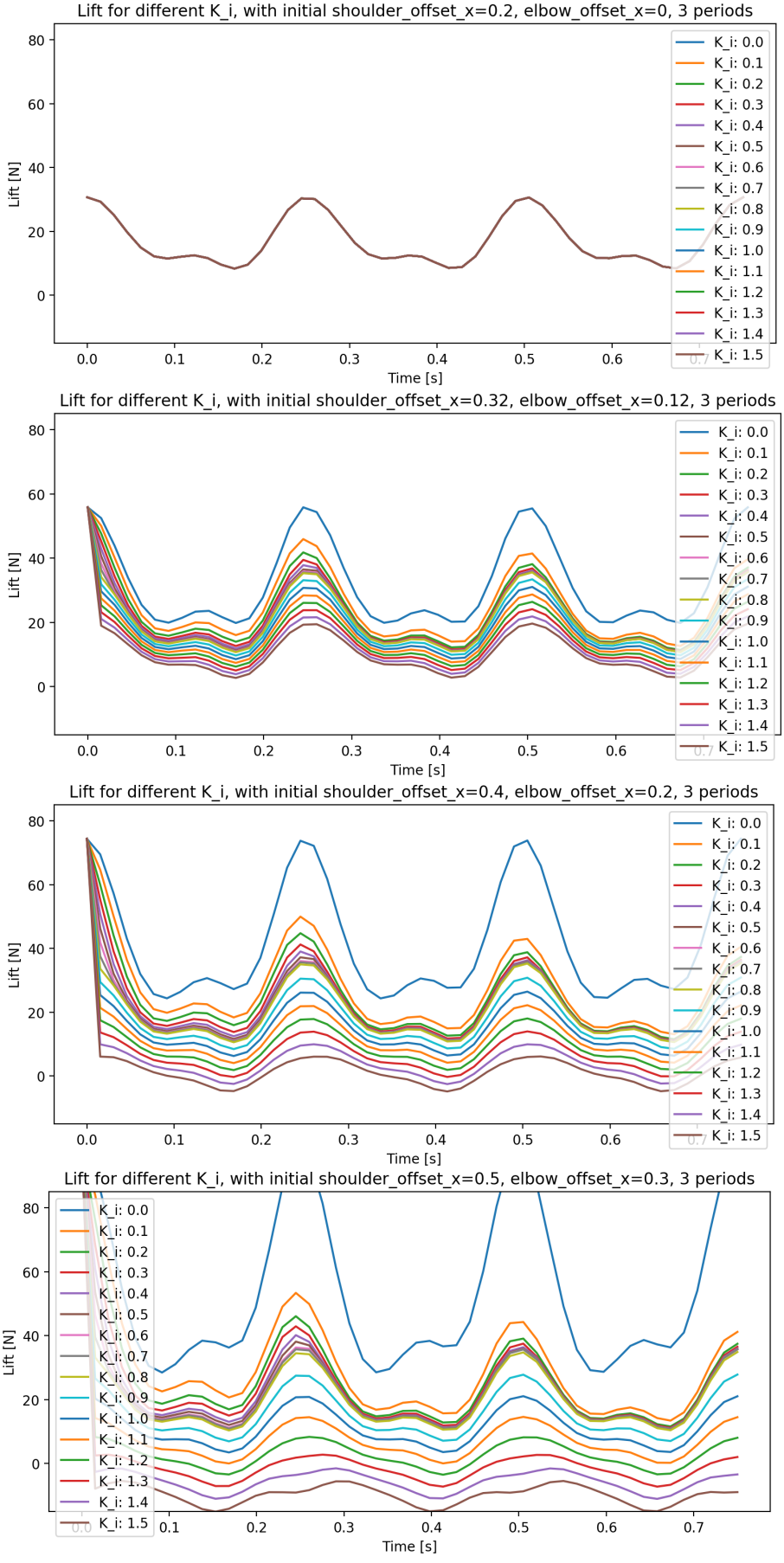


**Figure 6.8:** *Evolution of lift as a function of time for different integral gains $K_i$ with 3 flapping periods*

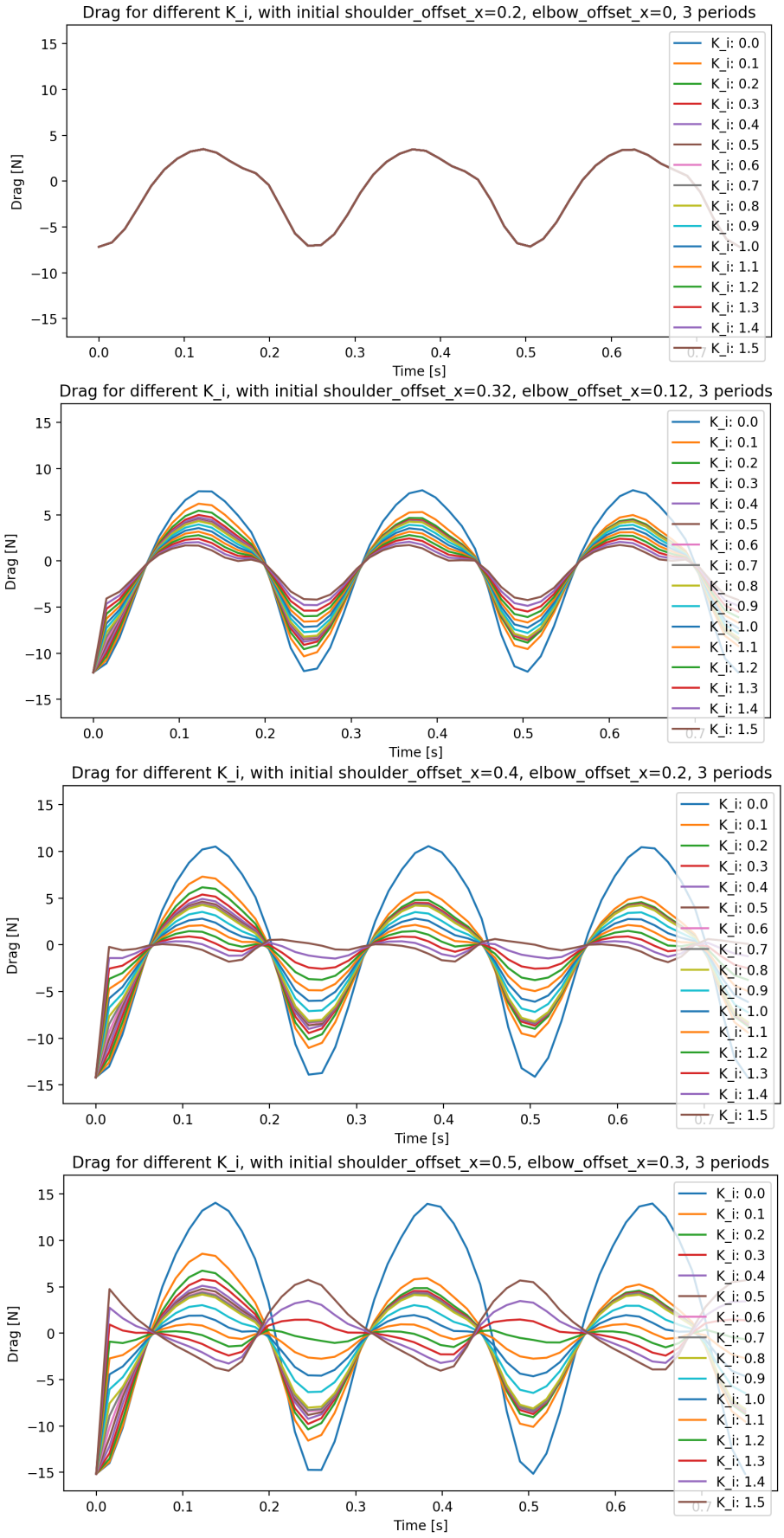


**Figure 6.9:** *Evolution of drag as a function of time for different integral gains $K_i$ with 3 flapping periods*

## 6.4 Arithmetic mean of lift and its derivative

The figures 6.10 and 6.11 represent the arithmetic mean of lift as a function of time for integral gains between 0 and 1.5. An integral gain equal to 0 is equivalent to the absence of a controller. The figure 6.10 represents 3 flapping periods, whereas the figure 6.11 represents 10 flapping periods.
The figures 6.12 and 6.13 represent the derivative of the arithmetic mean as a function of time for integral gains between 0 and 1.5. The figure 6.12 represents 5 flapping periods, whereas the figure 6.13 represents 10 flapping periods.

Each figure includes 4 graphs: the upper graph corresponds to a situation with no entrance in the stall area (the shoulder offset along the x axis is equal to 0.2 radians (approximately 11.5°) and the elbow offset along the x axis is equal to 0 radians (0°)).
The graph in second position corresponds to a situation with an initial low entrance in the stall area (the initial shoulder offset along the x axis is equal to 0.3 radians (approximately 17.2°) and the initial elbow offset along the x axis is equal to 0.1 radians (approximately 5.7°)).
The graph in third position corresponds to a situation with an initial medium entrance in the stall area (the initial shoulder offset along the x axis is equal to 0.4 radians (approximately 22.9°) and the initial elbow offset along the x axis is equal to 0.2 radians (approximately 11.5°)).
The graph at the bottom corresponds to a situation with an initial important entrance in the stall area (the initial shoulder offset along the x axis is equal to 0.5 radians (approximately 28.6°) and the initial elbow offset along the x axis is equal to 0.3 radians (approximately 17.2°)).

We can observe on figures 6.10 and 6.11 that the arithmetic mean of lift as a function of time converges towards the mean of lift for one flapping period. This indicates that the stabilisation value of the lift depends on the integral gain parameter. The greater the integral gain is, the lower the stabilisation value of the lift will be. This is due to the fact that an important reaction of the bird (represented by the controller) greatly reduces the angle of attack. Below the critical angle of attack, the lift coefficient increases with the angle of attack. If the bird greatly reduces its angle of attack, the lift decreases and it may become problematic if the lift is not sufficient to compensate the bird's weight.

We can observe on figures 6.12 and 6.13 that the derivative of the arithmetic mean of lift is a sinusoid whose amplitude decreases over time. Each cycle of the sinusoid is representative of one flapping period. The greater the integral gain is, the greater the amplitude of the sinusoid is (except for $K_i = 0$ which represents the absence of a controller). It means that the greater the integral gain is, the greater the impact on the decrease of lift will be.

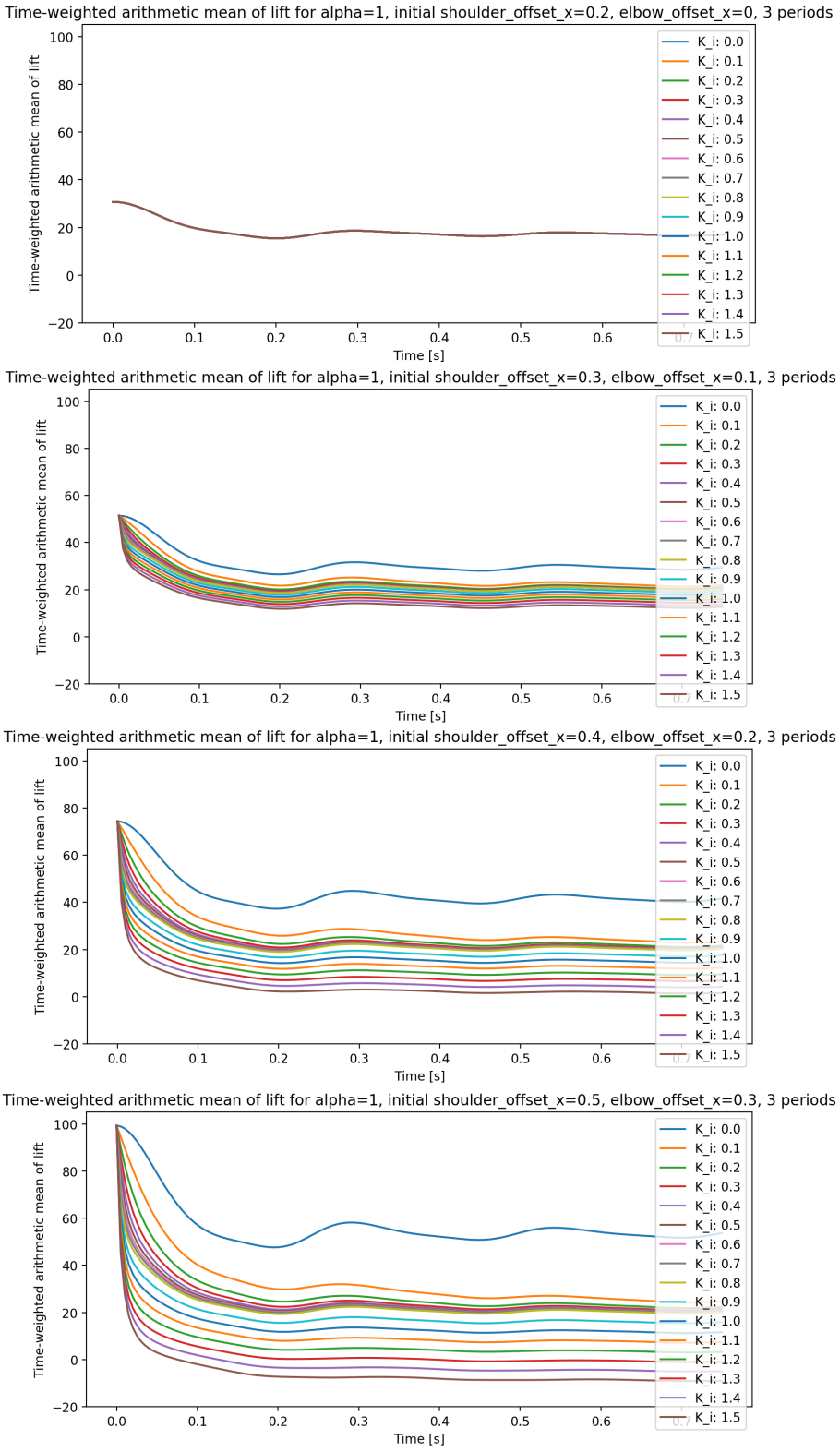


**Figure 6.10:** *Arithmetic mean of lift for different integral gains $K_i$ with 3 flapping periods*

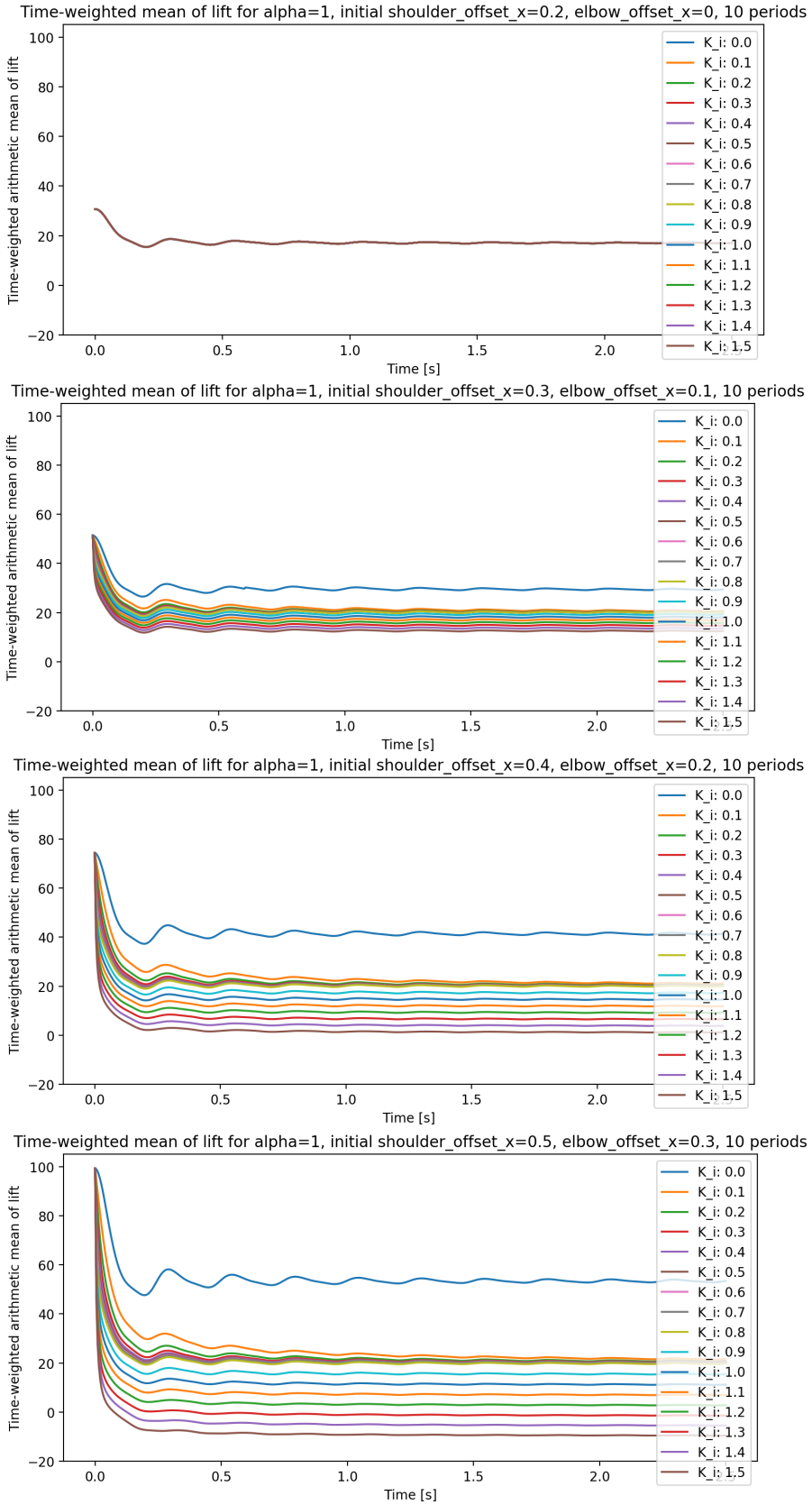


**Figure 6.11:** *Arithmetic mean of lift for different integral gains $K_i$ with 10 flapping periods*

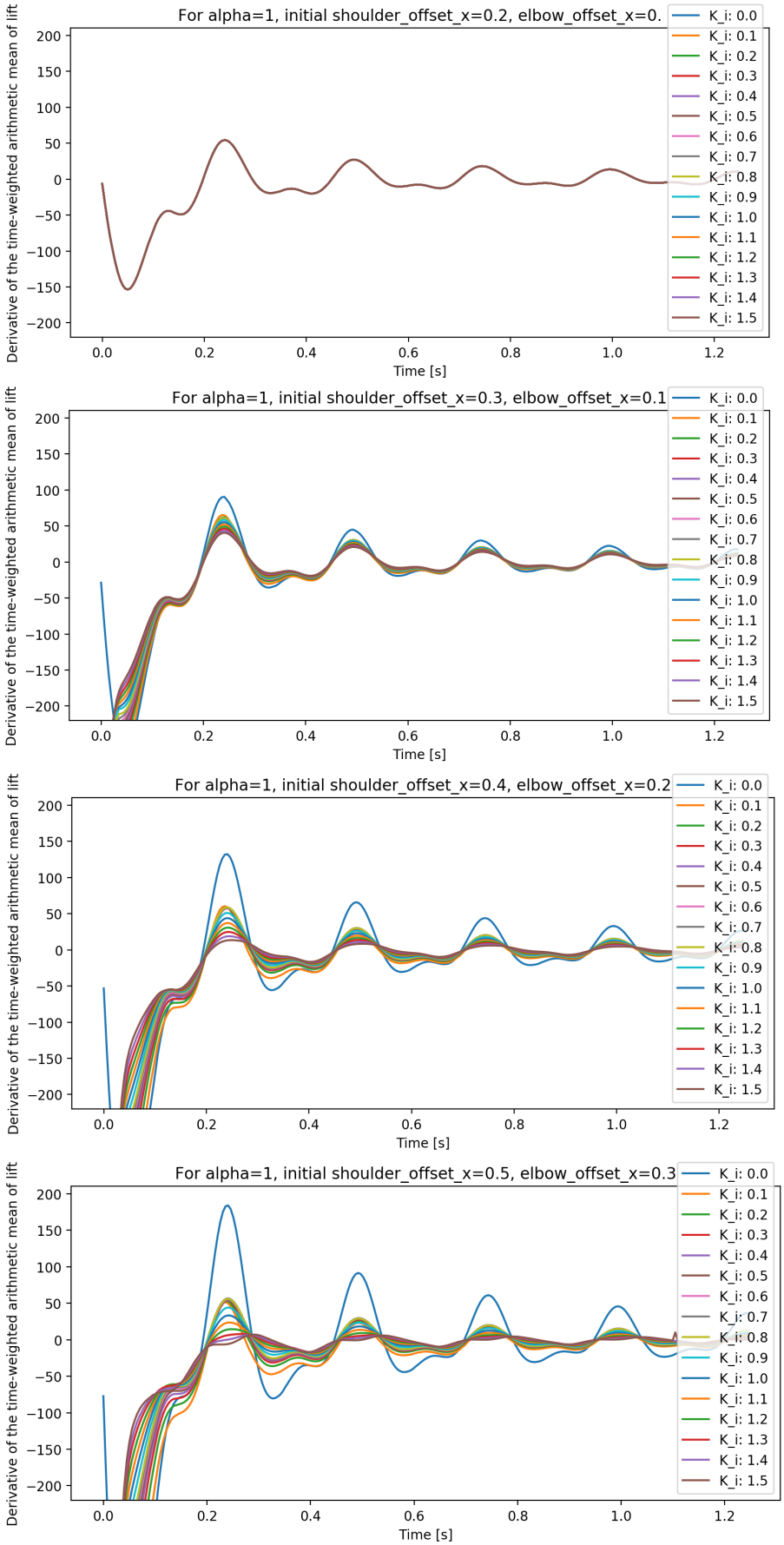


**Figure 6.12:** *Derivative of the arithmetic mean of lift for different integral gains $K_i$ with 5 flapping periods*

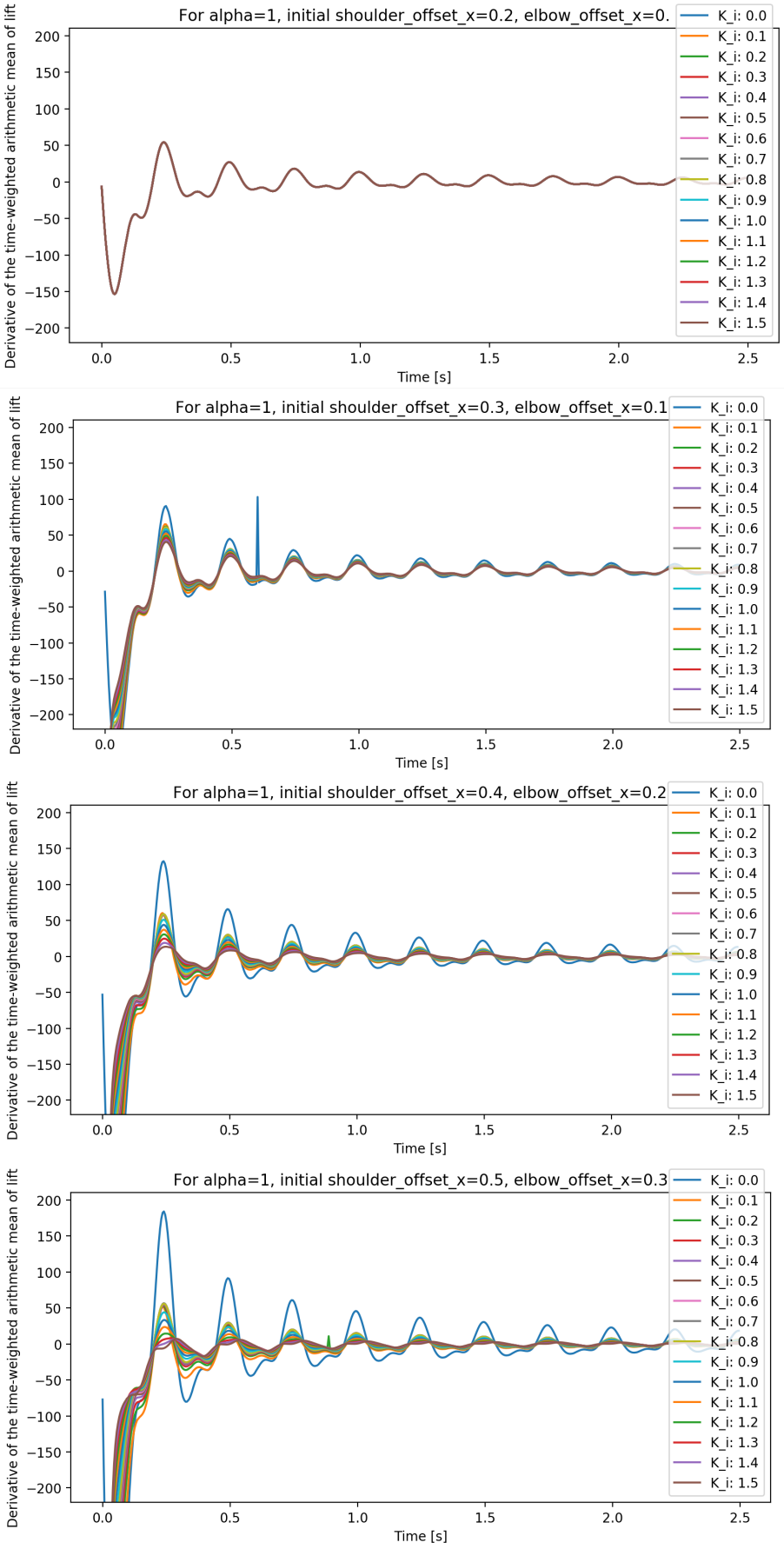


**Figure 6.13:** *Derivative of the arithmetic mean of lift for different integral gains $K_i$ with 10 flapping periods*

## 6.5 Shoulder and elbow offsets along the x axis

The figure 6.14 represents the evolution of the offset of the harmonic trajectory of the shoulder along the x axis as a function of time for integral gains between 0 and 1.5, during 3 flapping periods.
The figure 6.15 represents the evolution of the offset of the harmonic trajectory of the elbow along the x axis as a function of time for integral gains between 0 and 1.5, during 3 flapping periods.
An integral gain equal to 0 is equivalent to the absence of a controller.
(We consider the frame presented in figure 4.2 as the reference frame.)

Each figure includes 4 graphs: the upper graph corresponds to a situation with no entrance in the stall area (the shoulder offset along the x axis is equal to 0.2 radians (approximately 11.5°) and the elbow offset along the x axis is equal to 0 radians (0°)).
The graph in second position corresponds to a situation with an initial low entrance in the stall area (the initial shoulder offset along the x axis is equal to 0.3 radians (approximately 17.2°) and the initial elbow offset along the x axis is equal to 0.1 radians (approximately 5.7°)).
The graph in third position corresponds to a situation with an initial medium entrance in the stall area (the initial shoulder offset along the x axis is equal to 0.4 radians (approximately 22.9°) and the initial elbow offset along the x axis is equal to 0.2 radians (approximately 11.5°)).
The graph at the bottom corresponds to a situation with an initial important entrance in the stall area (the initial shoulder offset along the x axis is equal to 0.5 radians (approximately 28.6°) and the initial elbow offset along the x axis is equal to 0.3 radians (approximately 17.2°)).

For all figures of the results chapter, a difference of 0.2 radians was set between the shoulder offset and the elbow offset as it is a common angular difference. Given that accurate geometric data about bird flight currently do not exist in scientific literature and are quite difficult to obtain experimentally, this angular difference is an assumption that could not be verified.

We can observe on figures 6.14 and 6.15 that the greater the integral gain is, the more the shoulder offset and the elbow offset along the x axis will decrease. We can also see that the adjustment of the shoulder offset and of the elbow offset by the controller is instantaneous for integral gains between 0.8 and 1.5 and takes a variable time for integral gains between 0.1 and 0.7. This adjustment time increases if the integral gain is reduced.

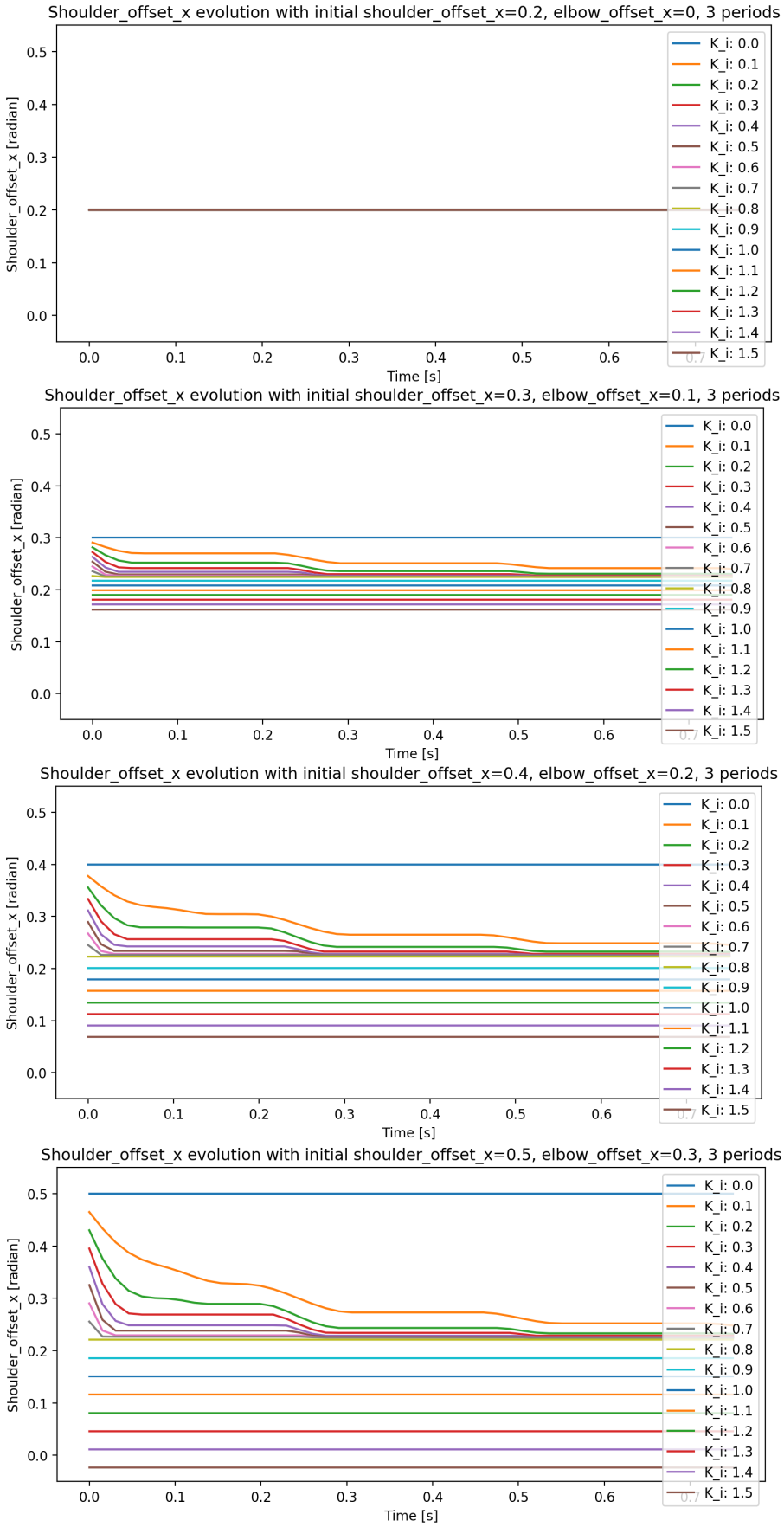


**Figure 6.14:** *Evolution of the offset of the harmonic trajectory of the shoulder along the x axis as a function of time for different integral gains $K_i$ with 3 flapping periods*

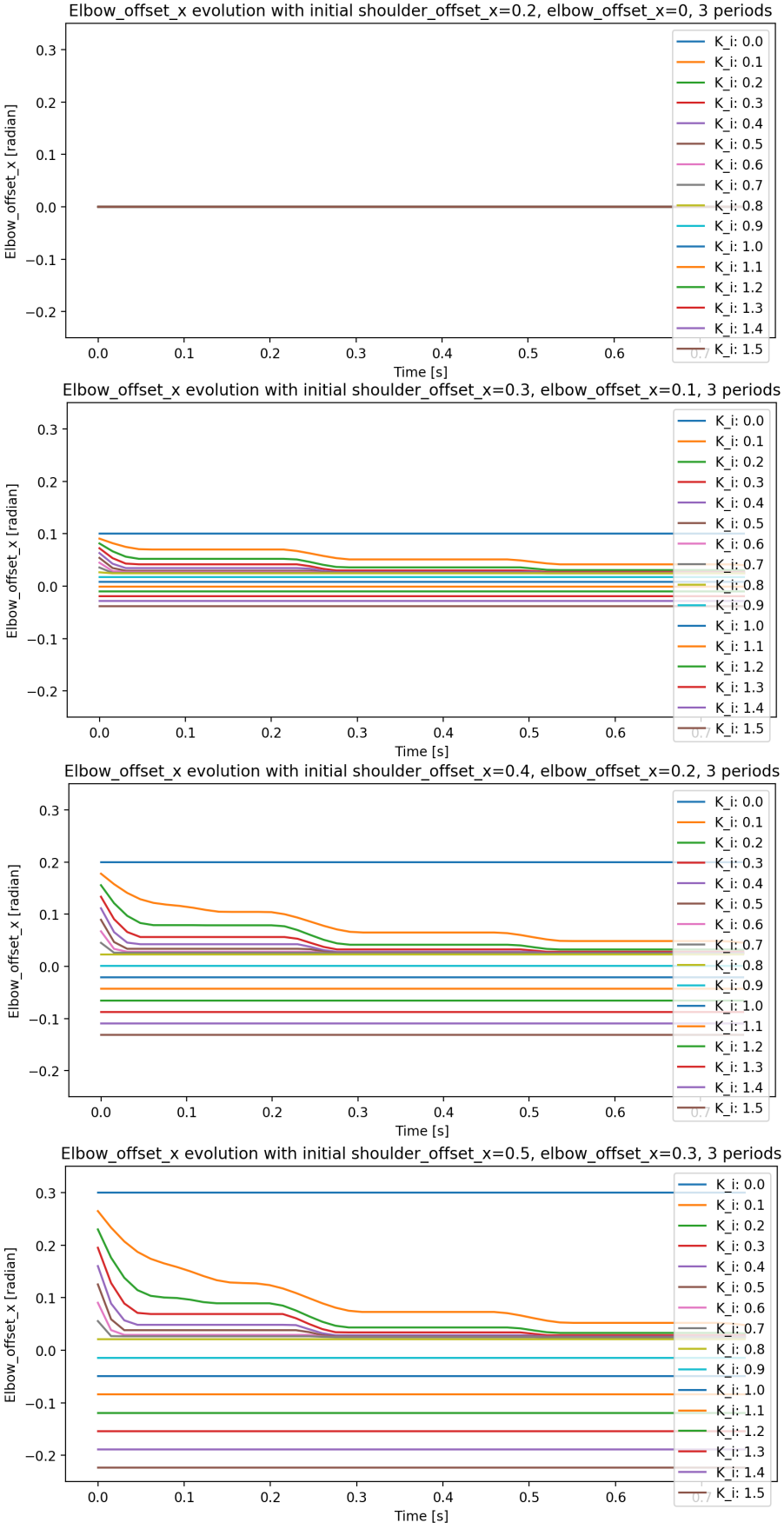


**Figure 6.15:** *Evolution of the offset of the harmonic trajectory of the elbow along the x axis as a function of time for different integral gains $K_i$ with 3 flapping periods*

# 7 Discussion

## 7.1 General discussion

Choosing a controller and its gain often involves a compromise. In order to make this compromise, there are 3 parameters to consider: the response time of the controller, the quality of the controller response (if there is stabilisation of the response and if the stabilisation values are interesting) and the impact of singular values of the bird model on the controller response.

### 7.1.1 Response time of the controller

We saw in the previous chapter that the response time of the controller decreases when the integral gain increases. In particular, we observed on the graphs of the shoulder and elbow offsets evolution (figures 6.14 and 6.15) that the adjustments of the shoulder offset and of the elbow offset seem to be instantaneous for integral gains above 0.8 and take a variable time for integral gains below 0.8. We also observed on the mean angle of attack graphs (figures 6.5 and 6.6) that the stabilisation of the angle of attack below the 15° threshold has an order of magnitude of 100 to 150 ms for integral gains between 0.9 and 1.5, whereas the stabilisation is longer and takes a duration which is more complex to compute (because of the periodic proximity to the 15° stall threshold) for integral gains below 0.9.

To stabilise the bird flight, it is necessary to react quickly when stall onset is detected. Thus, a fast response is necessary. However, a too high integral gain implies a risk to generate a significant oscillation leading to instability. Therefore, there is a compromise to make between a controller with a small response time and an integral gain which does not risk to make the kinematics unstable.

### 7.1.2 Quality of the controller response

On the mean angle of attack graphs (figures 6.5 and 6.6), we observed that the curves for integral gains below 0.9 almost merge and become periodically very close to the 15° stall threshold (at the point of the flapping cycle for which the wing is at the upper position). This periodic proximity to the 15° stall threshold may induce instability. Therefore, it seems adequate to choose an integral gain superior or equal to 0.9.

We observed on the graphs of the arithmetic mean of lift (figures 6.10 and 6.11) that the greater the integral gain is, the lower the stabilisation value of the lift will be. A too low value of lift is problematic, because the lift needs to compensate the bird's weight (which is approximately equal to 11.8 N for the bird model) to avoid a loss of altitude. On the graph of the lift evolution as a function of time (figure 6.8), we saw that for the situation with an important entrance in the stall area, the lift curves for integral gains above 1.1 are not sufficient to compensate the bird's weight. Thus, the integral gain of the controller should be lower than 1.1.

### 7.1.3 Impact of singular values on the controller response

The bird model simulation sometimes presents singular values at some points of the computation, this explains the presence of irregular spikes for certain integral gains in some graphs of the results chapter. These singular points are not representative of the reality. If the integral gain of the controller is too high, there is a risk of instability if, for a certain time step, the angle of attack value is much higher than the 15° threshold because of a singular value of the simulation.

Therefore, we suggest the compromise of an integral controller with an integral gain between 0.9 and 1.1.

## 7.2 Limits of the study

A major drawback of this study is that the reactions implemented in the controller are based on realistic assumptions that could not be verified with certainty. This is due to the absence of accurate studies on bird morphologies in the scientific literature. How birds move their wings in flight is not known with accuracy.

A second important drawback is the presence of singular values in the bird model which interferes with the relevance of certain results.

In addition, we made the simplifying assumptions that there is no loss of sensory data when the information is transmitted from the sensory receptors to the integrating centre and that the value of this sensory data (giving an indirect idea of the angle of attack) is correct. We also made the simplifying hypothesis that the controller receives this sensory data instantaneously. (There is information about the reaction time of sensory receptors in Appendix A that was not used for this model but that might be relevant for future studies.) To have more accurate results, the sensory receptors should have been modelled.

Furthermore, the compliance of the wing is not investigated in this master thesis, but might have a beneficial effect mitigating the perturbations due to stall onset and on the wing adjustments made by the controller.

Moreover, the controller implemented in this master thesis only limits high angles of attack but does not take into account the risk of dynamic stall. The dynamic stall is a non-linear aerodynamic effect that occurs when the angle of the attack of the airfoil rapidly changes. This rapid change can cause a strong vortex that comes from the leading edge and travels above the wing, this briefly increases the lift and then, reduces it dramatically. [35]

## 7.3 Future perspectives

Biologically, it would be interesting to model the reaction time of the sensory receptors. The risk of sensory data loss and the risk of incorrect sensory data due to external perturbations could also be investigated in a study that would focus more on sensory receptors.

In terms of control, the analysis of the controller would be more thorough if the controller response times could be computed.

In terms of aerodynamics, it could be insightful to implement the controller in a bird model without the hypothesis of imposed kinematics. This would permit to take into account the effects of aerodynamic turbulence. In addition, the kinematics of the bird would be able to adapt according to the flight conditions.
The compliance of the wing could also be investigated, to better represent the bird's adaptation to flight conditions.
The effect of dynamic stall could be investigated in order to take into account an other type of stall onset that often affects flapping flight.

# 8 Conclusion

Birds have impressive flight capabilities which could be a source of inspiration for new aerial vehicles. Their impressive flight capabilities are, in particular, an excellent manoeuvrability, a high adaptability to environment changes and a good capacity of minimisation of energy costs in flight (which gives them a very good endurance).

The main goal of this master thesis was to design a controller to stabilise the flight of a bird model by stopping the stall onset when stall is detected by the sensory receptors. One main difficulty was the multidisciplinary aspect, that is to have a general view of the problem dealing with aerodynamics, control and biology.
The second main difficulty was to select a relevant level of modelling. A model cannot represent its subject in a perfectly realistic way. A suitable level of modelling had to be chosen in order to obtain the desired results, without making the model unnecessarily complex.

Here is a brief summary of this master thesis:
First, we identified the relevant sensory receptors to detect the stall onset. These sensory receptors are the mechanoreceptors located within the supporting tissues of the alula joint and in the covert feathers of the dorsal wing (responsible for detecting elevation of feathers, that is stall onset when the elevation is sufficiently important).
Then, the bird model, its hypotheses and its limits were presented.
Next, the controller was designed. Firstly, the condition for which the bird is subjected to stall was defined. Secondly, the flight parameters that needed to be changed for the bird to stop stalling were identified. Thirdly, it was chosen to design an integral controller.
After that, an interval for the integral gain was selected based on the graphs of the mean angle of attack, of the lift and its arithmetic mean, and of the shoulder and elbow offsets along the x axis.
Finally, the limits of the study and the future perspectives were discussed.

# A

# Reaction time of sensory receptors

Mechanisms of actions of sensory receptors are too different to make a general model. The only common points are that the action of the sensory receptor is interposed between the external stimulus (from the environment) and the initiation of the nerve impulse, and that the action of the sensory receptor includes the generation of an electrical potential. [36]

A general model of isolated sensory receptors has been designed with its primary afferent neuron. It is a model of information transmission and not a model of mechanisms of receptor action. The input is the intensity of the sensory signal (which can be chemical, optical, linked to pressure, temperature or pain). The output is the rate of neural impulse transmission in the afferent neuron. This model is based on the assumption that information is conserved when transmitted in a highly efficient sensory receptor. Thus, information transmitted by the stimulus is equal to information received by the system. [37]

However, this information transmission is not instantaneous, it takes a finite period of time. At the beginning of this period, the information lacks precision, because the receptor is uncertain about the intensity of the stimulus signal at the start, then it loses uncertainty and sends more precise information. Uncertainty can be considered as a monotone decreasing function of stimulus duration and a monotone increasing function of stimulus variance (spread of intensity values). The stimulus is defined as a signal with clearly defined statistical properties (for instance, the concentration of a solution for chemical sensory receptors). It is supposed to be sampled by the sensory receptor. [37]

This model is valid for both steady and time-varying signals. It has been shown that more intense stimuli are remembered by sensory receptors for longer periods of time than less intense stimuli. Indeed, more intense stimuli produce an expansion of local memory and less intense stimuli involve contraction of local memory. [37]

To be able to react to a stimulus, it is necessary to accumulate a quantum of information ($\Delta$H bits of information), this permits to compute the reaction time. The function $1 - exp^{-a \cdot t}$ corresponds to the rate at which a receptor samples its sensory stimulus. [37]

For a single step input, the information theoretical entropy, also called the uncertainty of sensory receptor about the intensity of the stimulus, is given by [37] :

$$H = \frac{1}{2} log(1 + \frac{\lambda}{1 - exp^{-a \cdot t}})$$

($\lambda$ and a are constant)

The information gained from the stimulus (thus transmitted by the sensory stimulus) is given by [37] :

$$I = H(t_0) - H(t_{max})$$

with $t_{max}$ : the time taken by the neuron to adapt to its equilibrium level

# Bibliography


[1] UCLouvain page on the RevealFlight Project https://sites.uclouvain.be/RevealFlight/project. Accessed 15 Fev. 2020

[2] Code by Gianmarco Ducci, PhD student at Ecole Polytechnique de Louvain https://github.com/vortexlab-uclouvain/multiflap

[3] Thomas Heinbockel *Introductory Chapter: Organization and Function of Sensory Nervous Systems, Sensory Nervous System.* July 2018

[4] Michael Rubin *Overview of the Peripheral Nervous System* MSD Manual Consumer Version Center, consulted on the 19/02/21

[5] Alessandro Santuz *Extracting muscle synergies from human steady and unsteady locomotion: methods and experiments* Thesis, DO : 10.18452/19351, August 2018

[6] Douglas L. Altshuler, Joseph W. Bahlman, Roslyn Dakin, Andrea H. Gaede, Benjamin Goller, David Lentink, Paolo S. Segre, Dimitri A. Skandalis *The biophysics of bird flight: functional relationships integrate aerodynamics, morphology, kinematics, muscles, and sensors.* Canadian Journal of Zoology, October 2015.

[7] R. Brown, M. Fedde *Airflow sensors in the avian wing* The Journal of Experimental Biology 179, 13-30 (1993)

[8] Michael Gewecke, Martin Woike *Breast Feathers as an Air-current Sense Organ for the Control of Flight Behaviour in a Songbird (Carduelis spinus)* Ethology 47(3):293-298, April 2010

[9] Wolfgang Hörster *Histological and electrophysiological investigations on the vibration-sensitive receptors (Herbst corpuscles) in the wing of the pigeon (Columba livia)* Journal of Comparative Physiology A, volume 166, pp 663–673 (1990)

[10] Wolfgang Hörster *Vibrational sensitivity of the wing of the pigeon (Columba h'via) - a study using heart rate conditioning* Journal of Comparative Physiology A volume 167, pages545–549 (1990)

[11] Dale Crane *Dictionary of Aeronautical Terms, third edition* Aviation Supplies & Academics, page 486, 1997

[12] Lee Sang-im, Kim Jooha, Park Hyungmin, Piotr G. Jabłoński, Choi Haecheon *The Function of the Alula in Avian Flight* Scientific Reports volume 5, Article number: 9914 (2015)

[13] E.E. Ruppert, R.S. Fox, R.D. Barnes *"Annelida". Invertebrate Zoology (7 ed.)* Brooks / Cole. pp. 414–420, 2004

[14] Robert W. Storer *https://www.britannica.com/animal/bird-animal/Classification* Encyclopædia Britannica, Distinguishing taxonomic features, consulted the 02/02/21

[15] Reinhold Necker *Observations on the function of a slowly-adapting mechanoreceptor associated with filoplumes in the feathered skin of pigeons* Journal of Comparative Physiology A volume 156, pages 391–394 (1985)

[16] D.A. Sibley *The Sibley Guide to Birds* pp 85, 2000

[17] D. R. Warrick, M. W. Bundle, K. P. Dial *Bird maneuvering flight: blurred bodies, clear heads* Integrative and Comparative Biology, Vol. 42, No. 1, pp. 141-148, February 2002, Published by Oxford University Press

[18] D. Bilo, A. Bilo *Wind stimuli control vestibular and optokinetic reflexes in the pigeon* The Science of Nature 65(3):161-162, January 1978

[19] Semm, P., Beason, R.C. *Sensory basis of bird orientation* Experientia 46, 372–378 (1990).

[20] Martin, G.R. *Martin, G.R. Through birds' eyes: insights into avian sensory ecology* J Ornithol 153, 23–48 (2012)

[21] Andrew Burton, John Radford *Thinking in Perspective : Critical Essays in the Study of Thought Processes* Routledge, 1978, page 232, 1978

[22] Partha S. Bhagavatula, Charles Claudianos, Michael R. Ibbotson, Mandyam V. Srinivasan *Optic Flow Cues Guide Flight in Birds* Current Biology, Volume 21, Issue 21, pp 1794-1799, November 2011

[23] Rachel Muheim, Heiko Schmaljohann, Thomas Alerstam *Feasibility of sun and magnetic compass mechanisms in avian long-distance migration* Muheimetal.MovementEcology (2018) 6:8

[24] Melvin L. Kreithen, William T. Keeton *Detection of Changes in Atmospheric Pressure by the Homing Pigeon, Columba livia* Journal of Comparative Physiology, Volume 89, pp 73-82 (1974)

[25] A. W. Sherwood *Aerodynamics* pp. 102-105, London: McGraw Hill, 1946

[26] Jeremy M. V. Rayner *Flight adaptations in vertebrates, in Vertebrate Locomotion*, Symposia of the Zoological Society of London, Volume 48, pp. 137–169. London: Academic Press, 1981

[27] Christina Harvey *Gull wing morphing allows active control of trade-offs in efficiency, maneuverability and stability* Thesis, March 2018

[28] Bret W. Tobalske, Jason W. D. Hearn, Douglas R. Warrick *Aerodynamics of intermittent bounds in flying birds* Experiments in Fluids, January 2010.

[29] David Lentink, Andreas F. Haselsteiner, Rivers Ingersoll *In vivo recording of aerodynamic force with an aerodynamic force platform: From drones to birds* Journal of the Royal Society, September 2014.

[30] Kristen E. Crandell, Bret W. Tobalske *Kinematics and aerodynamics of avian upstrokes during slow flight* Journal of Experimental Biology, June 2015

[31] Gianmarco Ducci, Victor Colognesi, Gennaro Vitucci, Philippe Chatelain, Renaud Ronsse *Stability and sensitivity analysis of bird flapping flight* Journal of Nonlinear Science, Volume 31, Article 47, 2021

[32] Picture of a stork in flight from a RTFB article *https://ds1.static.rtbf.be/article/image/1920xAuto/c/1/6/297c3e0524044f93a9cf8f6fbee17f31-1434615604.jpg*

[33] Schematics of the angle of attack from an article about airfoil terminology from the the aviationchief website *http://www.aviationchief.com/uploads/9/2/0/9/92098238/airfoil-terminology-2.png*

[34] R. H. J. Brown *The flight of birds* Biological Reviews, Volume 38, 1963

[35] A. J. Buchner, J. Soria *Measurements of the flow due to a rapidly pitching plate using time resolved high resolution PIV* Aerospace Science and Technology, Volume 44, pages 4–17, 2015

[36] Davis Hallowell *Some Principles of Sensory Receptor Action* Physiological Review, Volume 41, Issue 2, April 1961

[37] Kenneth H. Norwich, Willy Wong *A universal model of single-unit sensory receptor action* Mathematical Biosciences, Volume 125, Issue 1, pages 83-108, January 1995

**UNIVERSITÉ CATHOLIQUE DE LOUVAIN**
**École polytechnique de Louvain**
Rue Archimède, 1 bte L6.11.01, 1348 Louvain-la-Neuve, Belgique | **www.uclouvain.be/epl**